

# **Supplementary Information:**

## **Reduced False Positives in Autism Screening Via Digital Bio-markers Inferred from Deep Co-morbidity Patterns**

Dmytro Onishchenko<sup>a</sup>, Yi Huang<sup>a</sup>, James van Horne<sup>a</sup>, Peter J. Smith<sup>d,g</sup>, Michael M. Msall<sup>e,f</sup>, Ishanu Chattopadhyay<sup>a,b,c,\*</sup>

<sup>a</sup>*Department of Medicine, University of Chicago, Chicago, IL, USA*

<sup>b</sup>*Committee on Genetics, Genomics & Systems Biology, University of Chicago, Chicago, IL, USA*

<sup>c</sup>*Committee on Quantitative Methods in Social, Behavioral, and Health Sciences, University of Chicago, Chicago, IL, USA*

<sup>d</sup>*Department of Pediatrics, Section of Developmental and Behavioral Pediatrics, University of Chicago, Chicago, IL, USA*

<sup>e</sup>*Department of Pediatrics, Section Chief of Developmental and Behavioral Pediatrics, University of Chicago, Chicago, IL, USA*

<sup>f</sup>*Joseph P. Kennedy Research Center on Intellectual and Neurodevelopmental Disabilities, University of Chicago, Chicago, IL, USA*

<sup>g</sup>*Executive Committee Chair, American Academy of Pediatrics' Section on Developmental and Behavioral Pediatrics*

---

## **Contents**

<b>1 Pipeline Optimization</b>	<b>16</b>
1.1 Input Data Format . . . . .	16
1.2 Algorithms . . . . .	16
<b>2 Example Run with Released Application</b>	<b>19</b>
2.1 Prerequisites & Installation . . . . .	19
2.2 EHR data format . . . . .	20
2.3 Sample Python code risk estimation . . . . .	20
2.4 Sample Python script risk estimation . . . . .	20
<b>3 Comparison With State of the Art Off-the-shelf ML Algorithms</b>	<b>20</b>
<b>4 Comparison With Pipeline Variations, Feature Subsets and Neural Net Post-processing</b>	<b>21</b>
4.1 Feature Subset Evaluations & Code Density As A Feature . . . . .	21
<b>5 Threshold Selection on ROC Curve</b>	<b>21</b>
<b>6 Note on Reciever Operating Characteristics (ROC) and Precision-recall Curves</b>	<b>22</b>
<b>7 Effect of Class Imbalance</b>	<b>23</b>
<b>8 Note on ASD Clinical Diagnosis &amp; Uncertainty of EHR Record</b>	<b>23</b>
8.1 Diagnostic Evaluations . . . . .	23

---

\*To whom correspondence should be addressed: e-mail: ishanu@uchicago.edu.

8.2 Change In Diagnostic Criteria for ASD, Inclusion of PDD, Asperger, and Disambiguation From Unrelated Psychiatric Phenotypes . . . . .	24
8.3 Performance Comparison With M-CHAT/F . . . . .	24
<b>9 Improving Wait-times For Diagnostic Evaluations by Reducing False Positives in Routine Screening</b>	<b>25</b>
9.1 4D Decision Optimization Using M-CHAT/F Population Stratification To Boost PPV . . . . .	25
<b>10 Generating PFSA Models From Set of Input Streams with Variable Input Lengths</b>	<b>26</b>
<b>11 Probabilistic Finite State Automata Inference</b>	<b>26</b>
11.1 Probabilistic Finite-State Automaton . . . . .	26
<b>12 Sequence Likelihood Defect</b>	<b>28</b>

SI-Table 1: Boosted Sensitivity, Specificity and PPV Achieved at **150 weeks** Conditioned on M-CHAT/F Scores

M-CHAT/F Outcome				global performance (Truven)			global performance (UCM)			prevalence
0-2 NEG	3-7 NEG	3-7 POS	$\geq 8$ POS	specificity	sensitivity	PPV	specificity	sensitivity	PPV	
specificity choices										
0.28	0.66	0.93	0.97	0.95	0.64	0.224	0.95	0.577	0.206	0.022
0.31	0.67	0.9	0.97	0.95	0.641	0.223	0.95	0.577	0.205	0.022
0.54	0.86	0.97	0.99	0.98	0.494	0.361	0.98	0.393	0.31	0.022
0.41	0.89	0.96	0.99	0.98	0.493	0.362	0.98	0.391	0.311	0.022
0.31	0.61	0.86	0.98	0.95	0.808	0.219	0.95	0.713	0.198	0.017
0.33	0.6	0.86	0.98	0.95	0.809	0.218	0.95	0.715	0.197	0.017
0.66	0.95	0.98	0.99	0.98	0.574	0.337	0.98	0.417	0.269	0.017
0.53	0.97	0.98	0.99	0.98	0.573	0.337	0.98	0.412	0.267	0.017
0.54	0.91	0.97	0.99	0.978	0.615	0.322	0.978	0.499	0.278	0.017
0.52	0.92	0.97	0.99	0.978	0.612	0.324	0.978	0.492	0.278	0.017

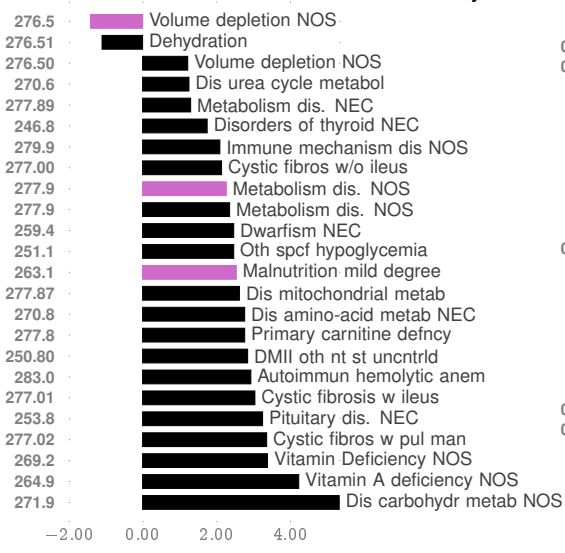
SI-Table 2: Population Stratification Results on large M-CHAT/F Study(n=20,375)<sup>1</sup>

<b>Id</b>	<b>Sub-population</b>	<b>Test Result</b>	<b>ASD positive</b>	<b>ASD Negative</b>	<b>Total %</b>
A	M-CHAT/F $\geq 8$	Positive	0.34%	0.64%	0.99%
B	M-CHAT/F $\in [3, 7]$	Positive (after follow-up)	0.52%	4.39%	4.91%
C	M-CHAT/F $\in [3, 7]$	Negative (after follow-up)	0.14%	3.1%	3.24%
D	M-CHAT/F $\in [0, 2]$	Negative	1.22%	89.63%	90.86%
Total %			2.23%	97.77%	100%

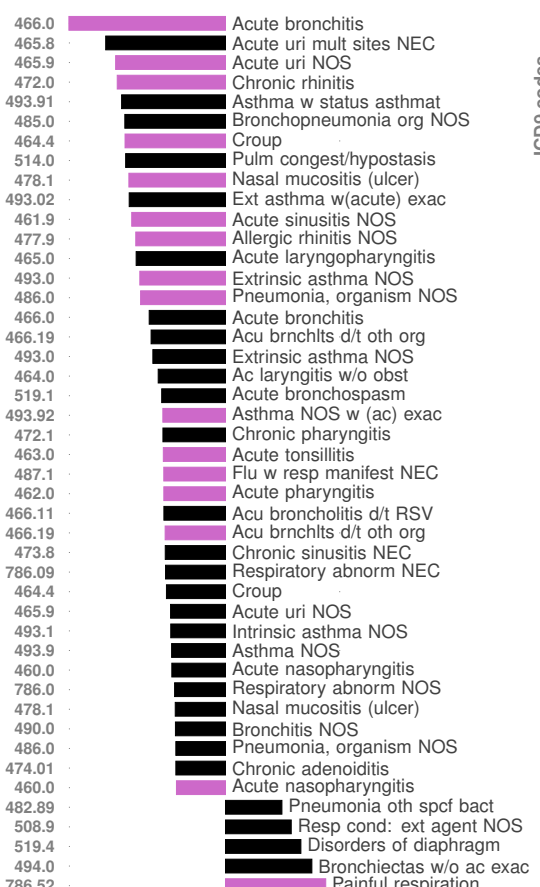
SI-Table 3:  $\gamma, \gamma'$  Computed from Population Stratification Recorded In M-CHAT/F Study<sup>1</sup> ( $\rho = 0.0223$ )

<b>Id</b>	<b>Sub-population</b>	<b>Test Result</b>	$\beta_i$	$\rho_i$	$\gamma_i$	$\gamma'_i$
A	M-CHAT/F $\geq 8$	Positive	.0099	.3469	.1540	.0066
B	M-CHAT/F $\in [3, 7]$	Positive (after follow-up)	.0491	.1059	.2331	.0449
C	M-CHAT/F $\in [3, 7]$	Negative (after follow-up)	.0324	.0432	.0627	.0317
D	M-CHAT/F $\in [0, 2]$	Negative	.9086	.0134	.5471	.9168

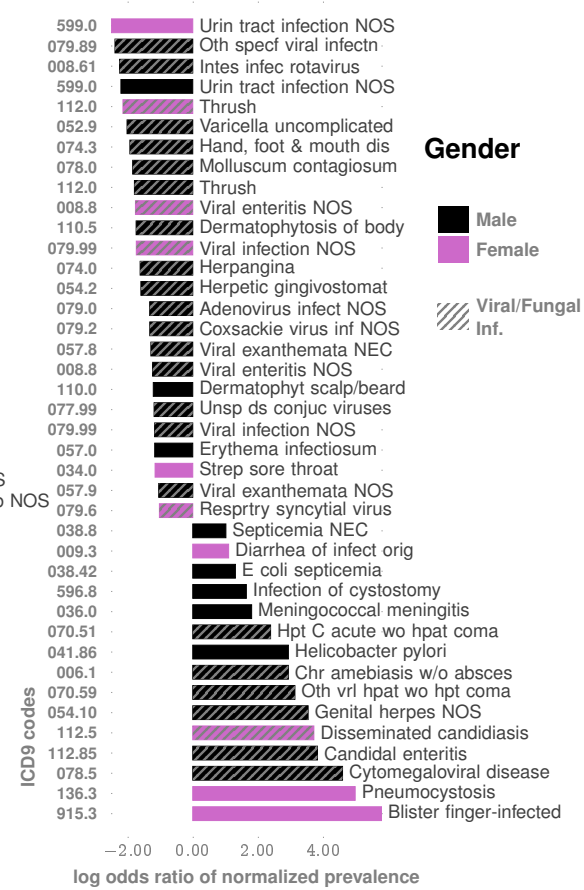
### A. Endocrine Nutritional Metabolic And Immunity Dis.



### B. Respiratory Disorders



### C. Infectious And Parasitic Diseases

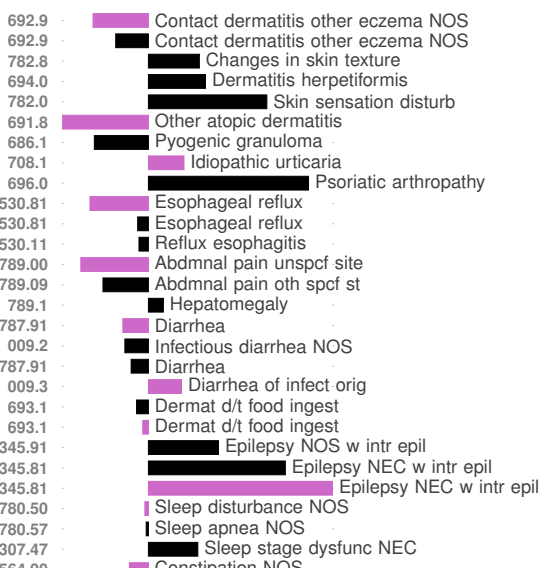


### Gender

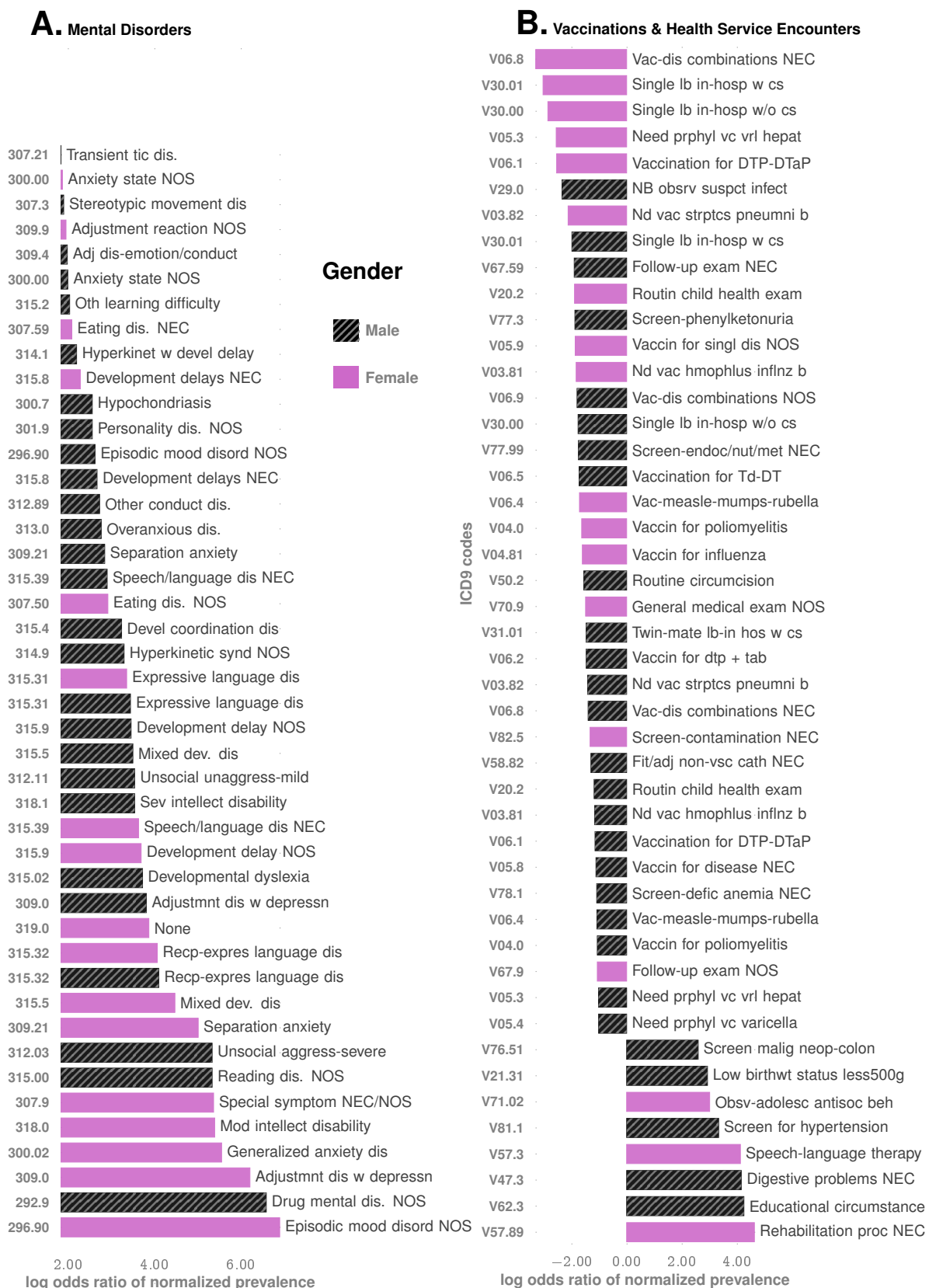
Male  
Female

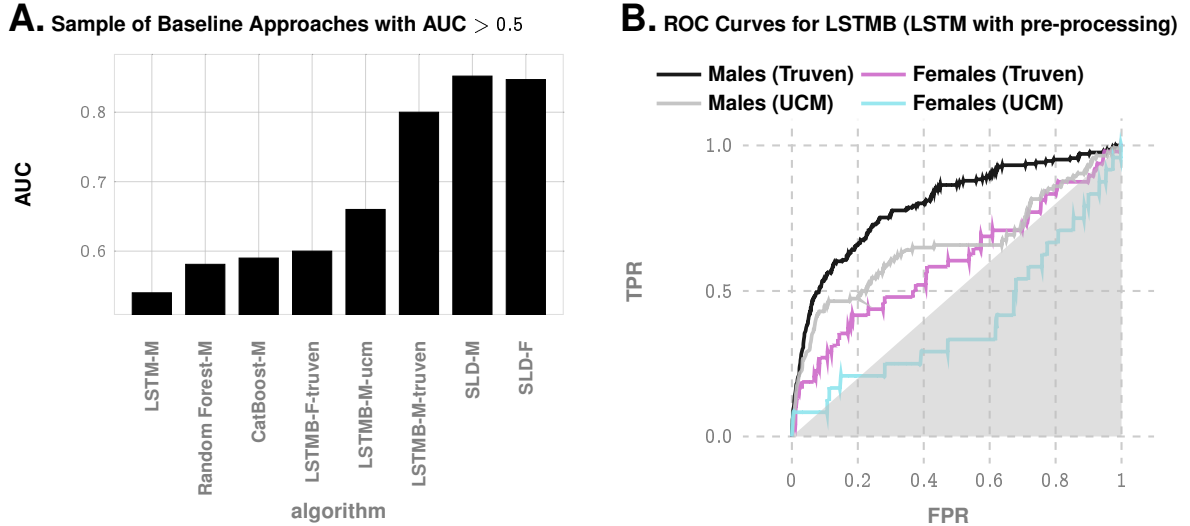
Viral/Fungal Inf.

### D. Similar Dis. with Opposed Association

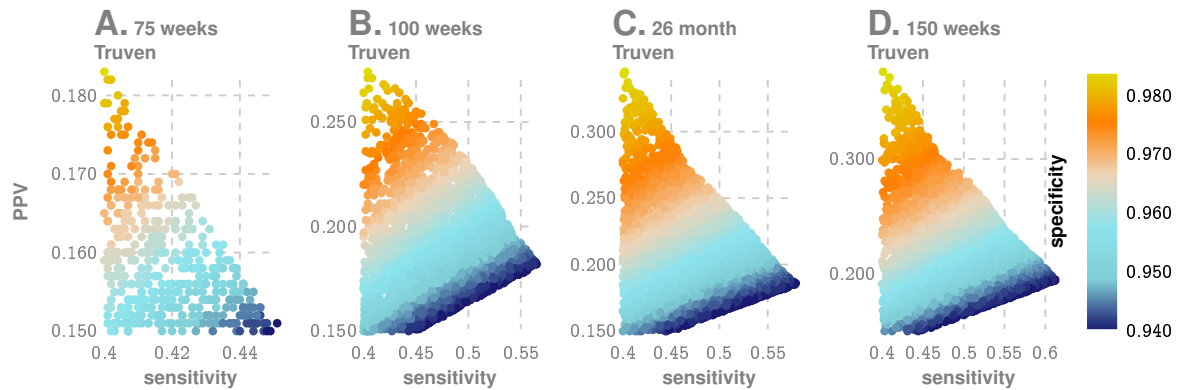


SI-Fig. 1: Details of Co-morbidity Patterns (at age < 3 years) for immunologic (panel A), respiratory (panel B), infections (panel C), and disorders with similar pathobiology manifesting opposing association with autism (panel D).

SI-Fig. 2: **Co-morbidity Patterns** for mental disorders, vaccinations and health-service encounters.

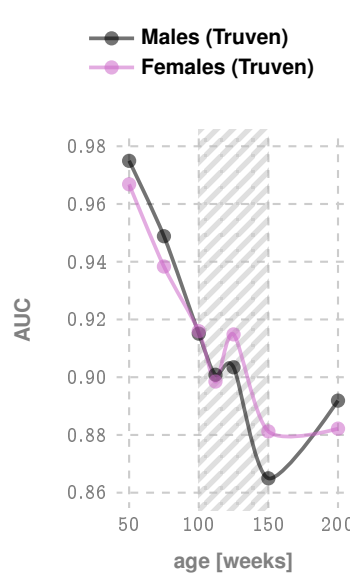


SI-Fig. 3: Performance of standard tools on correctly predicting eventual ASD diagnosis, computed at age 150 weeks of age. Long-short Term Memory (LSTM) networks are the state of the art variation of recurrent neural nets, and Random Forests and Gradient Boosting classifiers (CatBoost) are generally regarded as a representative state of the art classification algorithms. Sequence Likelihood Defect (SLD) is the approach developed in this study. LSTM-B denotes LSTM with identical pre-processing as in our pipeline (instead of using raw diagnostic codes). We get much better performance with LSTM-B with males in the Truven dataset, but the performance is sensitive to the sizes of the training set, and degrades for smaller samples available for females and in the UCM database, as shown in Panel B.

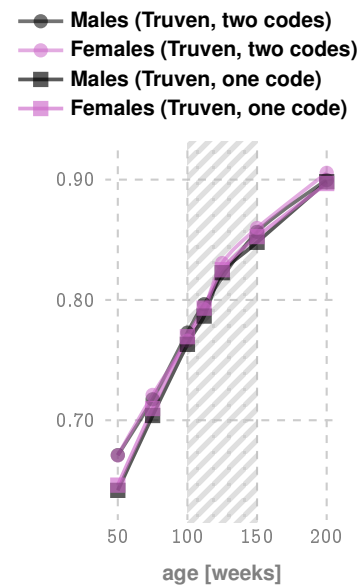


SI-Fig. 4: **4D Search To Take Advantage of Data on Population Stratification (Using Prevalence of 2.23% as reported by CHOP<sup>1</sup>).** While as a standalone tool our approach is comparable to M-CHAT/F at around the 26 month mark (and later), we can take advantage of the independence of the tests to devise a conditional choice of the operating parameters for the new approach. In particular, taking advantage of published estimated prevalence rates of different categories of M-CHAT/F scores, and true positives in each sub-population upon stratification, we can choose a different set of specificity and sensitivity in each sub-population to yield significantly improved overall performance across databases, and much earlier. Additionally, we can choose to operate at a high recall point, where we maximize overall sensitivity, or a high precision point, where we maximize the positive predictive value.

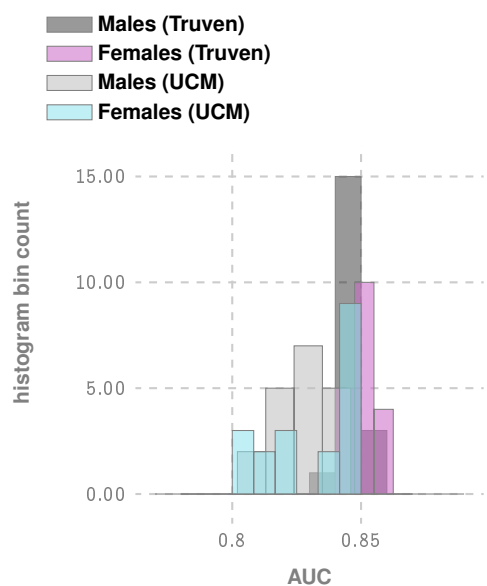
**A. Disambiguation of Autism Diagnosis from Other Psych. Phenotypes**



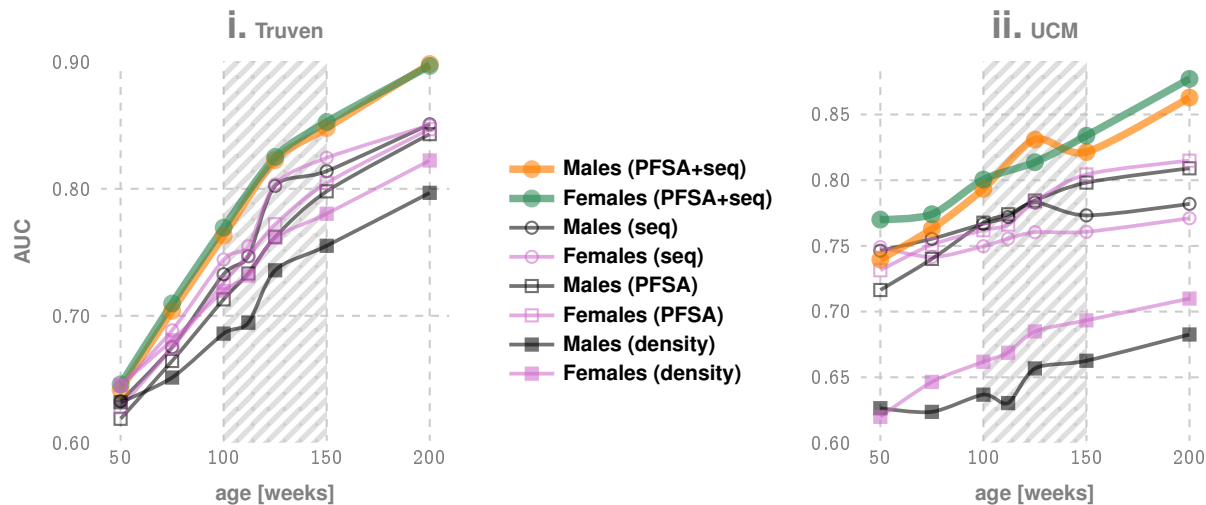
**B. Comparison of Performance with One vs Two ASD Diagnostic Codes**



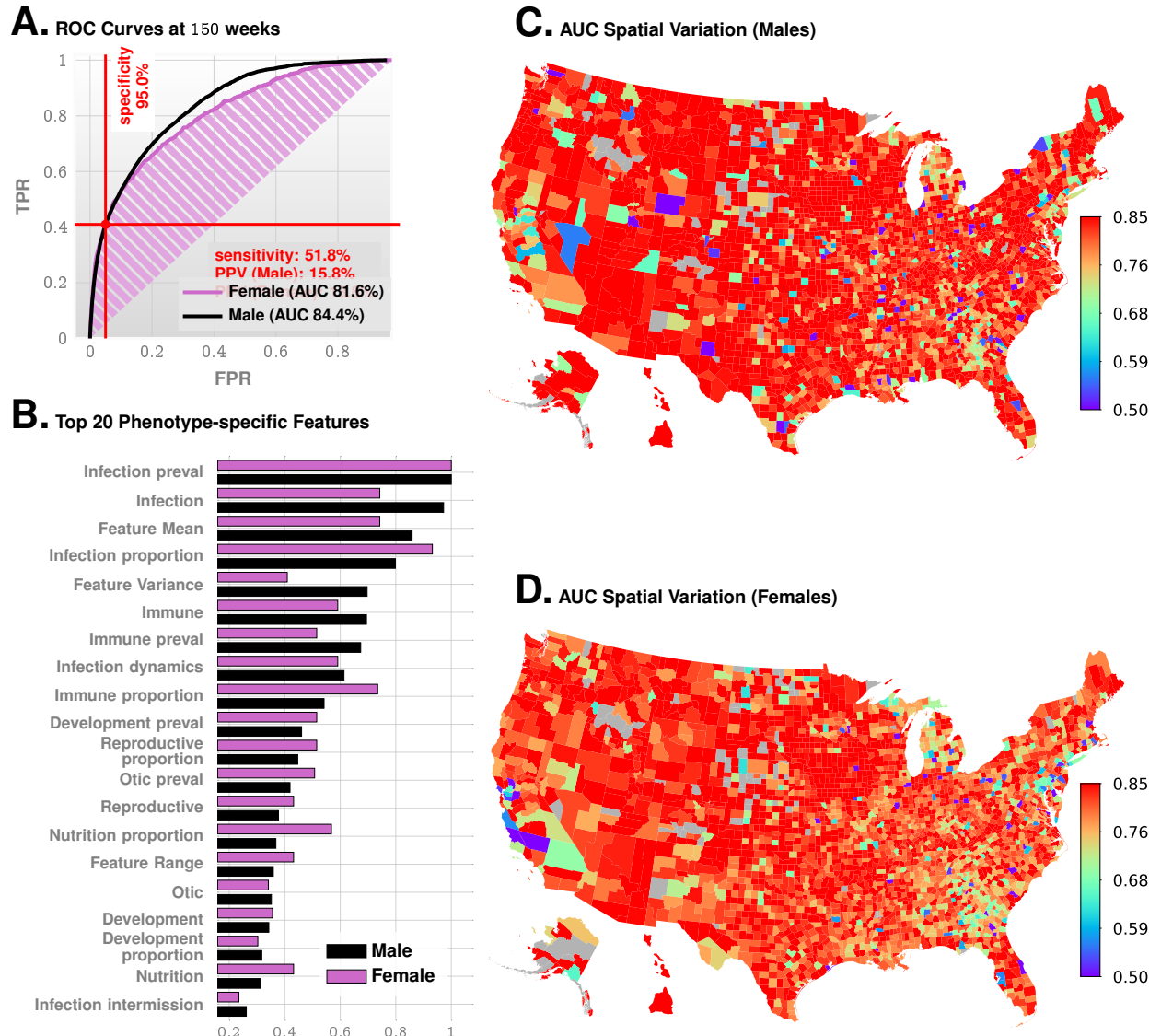
**C. AUC Distribution with Matched Control & Treatment Population Sizes**



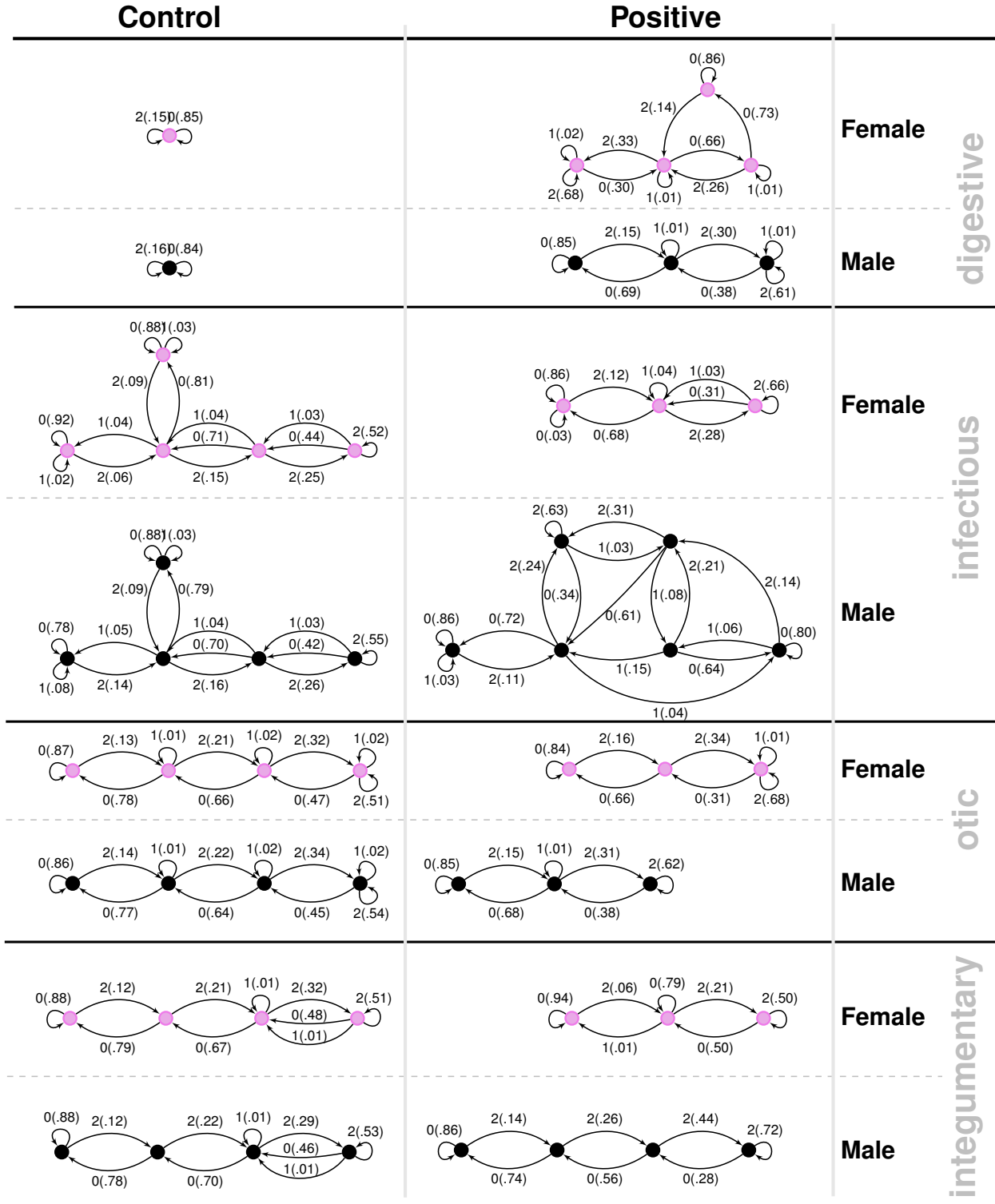
**D. Comparison of Performance with Different Feature Categories (Only PFSA based features, Only Sequence-statistics based features, only Code-density, and PFSA + Sequence-statistics features combined)**



**SI-Fig. 5: Evaluations of Feature Subsets, Class Imbalance, Code Density, Coding Uncertainty, & Disambiguation from Other Psychiatric Phenotypes.** Panel A illustrates that the pipeline performance where the control group is restricted to children to have at least one psychiatric phenotype other than ASD. It is clear that we have very good discrimination between ASD and non-ASD phenotypes. Panel B illustrates the situation where we restrict the treatment cohort to children to have at least 2 AD diagnostic codes, to see whether the pipeline performance is markedly different in populations where the coding errors/uncertainty is smaller. We see that such restrictions have no appreciable effect on pipeline performance. Panel C illustrates the AUC distributions obtained by using sampled control cohorts that are of the same size as the treatment cohort, to evaluate the effect of class imbalance. Again we see that such restrictions do not appreciably change performance. Panel D explores the performance changes when we use a restricted set of features, or simply use code density as the sole feature. We conclude that the combined feature set used in our optimized pipeline is superior to using the subsets individually. Code density is the least performant feature, and is not stable across databases.



SI-Fig. 6: Predictive Performance without psychiatric codes (ICD9 290 - 319) and codes for health status and services (ICD9 V0-V91) included. As shown, the performance is comparable at 150 weeks, with the AUC for females marginally lower (compare with Fig. 2 in the main text). The feature importances also are similar, with infectious diseases inferred to have the most importance (or weight) in the pipeline, which is also the case once we add psychiatric phenotypes, and codes for health services in our analysis. As shown in Fig. 2A, the psychiatric codes all increase risk, and the vaccination codes (See Fig. 2B) all decrease risk when those codes are included. This is why an alternate analysis was carried out to make sure that we are not picking up on psychiatric codes alone. Note in particular that the sensitivity/specificity point highlighted in panel A above is identical after adding the codes. This suggests that our predictive performance arises from patterns learned from co-morbidities, which are not just neuropsychiatric in nature.



SI-Fig. 7: Probabilistic Finite State Automata models generated for different disease categories for the control and positive cohorts. We note that in the first cases (digestive disorder), the models get more complex in the positive cohort, suggesting that the disorders become less random. However, in the categories of otic and integumentary disorders, the models become less complex suggesting increased independence from past events of similar nature. In case of infectious diseases, the model gets more complex for males, and less complex for females, suggesting distinct sex-specific responses associated with high ASD risk.

SI-Table 4: Disease Categories With Detailed Set of ICD9 Codes Used

Cat. †	Description	Constituent ICD9 Codes
Hematologic	Diseases Of The Blood And Blood-Forming Organs	286.9 286.7 286.6 283.19 283.10 283.11 283.9 283 283.1 284.9 284.8 284.81 284.0 284.89 284.09 284 284.01 282.2 287.49 287.41 287.39 287.4 287.5 287.32 287.3 287.30 287.31 286.3 286.2 286.1 286.0 286.4 282.1 282.6 282.5 282.41 282.42 282.68 282.69 282.62 282.63 282.60 282.61 282.64 282 282.8 287.33 281.2 281.3 280.0 282.9 285.8 285.9 280.9 284.2 285.1 285.2 285.3 280.1 285.22 285.21 282.3 776.5 285 283.0 285.29 280.8 282.7 282.40 282.49 284.1 284.19 284.12 284.11 281.8 281.9 281.4 281.0 281.1 286.5 287 287.8 287.9 287.2 287.0 287.1 285 289.52 289.50 289.51 289.59 289.4 289.5 289.81 289.83 289.82 289.89 289 289.7 289.8 289.9
Psychiatric	Mental Disorders (Except ASD)	290 through 319 (except 299.x)
Metabolic	Metabolic Disorders (Distinct from respiratory, digestive and immunological conditions)	273.4 270 270.2 270.3 712.11 712.10 712.13 712.12 712.15 712.14 712.17 712.16 712.19 712.18 712.31 712.30 712.37 712.36 712.35 712.34 712.38 712.33 712.32 712.28 712.29 712.24 712.25 712.26 712.27 712.20 712.21 712.22 712.23 712.39 712.1 712.3 712.2 277.6 275.1 277.85 277.87 270.7 270.6 276.6 276.4 276.2 276.3 276.0 275.41 276.1 276.8 276.9 276.69 275.5 275.42 271.1 330.2 272.7 271 274.89 712.85 274.82 712.99 712.98 274.01 274.00 274.03 274.02 712.91 712.90 712.93 712.92 712.95 712.94 712.97 712.96 712.88 712.89 274.10 274.11 712.82 712.83 712.80 712.81 712.86 712.87 712.84 274.19 712.9 712.8 274.0 274.1 274 274.8 274.9 271.2 275.01 270.5 270.4 278.8 272.3 275.03 275.09 271.3 272.6 272.5 278.1 271.8 277.5 263.0 263.2 262 260 261 263 263.1 269.8 269.9 263.8 263.9 269 277.7 272.2 330.3 271.9 275.40 272.8 277.8 275.49 275.2 277.88 275.4 269.3 275.9 275.8 277.9 277.89 251.2 251.1 251.0 278.01 278.00 278.03 270.8 270.9 278 278.0 278.02 277.86 270.1 275.3 277.1 277.81 277.82 272 272.1 277.2 272.4 272.9 273.9 273.8 268.1 265.2 268.0 268.2 268 265.0 265.1 266.1 266.0 266.2 266.9 264.3 264.2 264.1 264.0 264.7 264.6 264.5 264.4 264.9 264.8 268.9 267 266 265 264 269.2 269.0 269.1 278.2 278.3 278.4
Cardiovascular	Diseases Of Arteries, Arterioles, And Capillaries	442.89 441.6 442.84 442.82 442.83 442.8 441.03 441.02 441.01 441.00 441 414.19 414.12 442 414.10 414.11 447.70 447.71 447.72 447.73 414.1 442.81 441.9 442.1 442.0 442.3 442.2 441.2 441.3 441.0 441.1 442.9 441.7 441.4 441.5 437.3 447.7 443.29 443.23 443.22 443.21 443.24 443.2 444.9 444.8 444.81 444.2 444.1 444.0 444.89 444.444.22 444.21 445.81 440.31 440.30 440.32 414.01 414.00 414.03 414.02 414.05 414.04 414.07 414.06 445.89 411.81 445.02 445.01 440.24 440.22 440.23 440.20 440.21 440.445.40 429.40 414.0 414.2 440.4 440.3 440.2 440.1 440.0 440.9 440.8 445.8 445.0 414.3 414.4 426.54 426.52 426.51 426.50 426.13 426.12 426.11 426.10 426.89 426.9 426.8 426.81 426.3 426.2 426.1 426.0 426.7 426.6 426.5 426.4 427.61 427.60 427.5 427.89 427.69 427.32 427.41 427.9 427.81 427.8 427.42 427.6 427.4 427.31 427.2 427.3 427.0 427.1 425.8 425.9 425.4 425.7 425.0 425.1 425.2 425.3 346.6 438.51 438.52 438.53 438.50 290.4 431.0 438.42 438.41 438.40 432.9 290.43 290.42 290.41 402.0 426.0 426.12 426.11 426.10 426.89 426.9 426.8 426.81 426.3 426.2 426.1 426.0 426.7 426.6 426.5 426.4 427.61 427.60 427.5 427.89 427.69 427.32 427.41 427.9 427.81 427.8 427.42 427.6 427.4 427.31 427.2 427.3 427.0 427.1 425.8 425.9 425.4 425.7 425.0 425.1 425.2 425.3 436.6 438.51 438.52 438.53 438.50 290.4 431.0 438.42 438.41 438.40 432.9 290.43 290.42 290.41 433.91 433.90 430.0 434.10 434.11 434.1 438.21 438.20 438.22 433.20 433.21 438.6 438.7 438.11 438.12 438.13 438.14 438.19 433.31 433.30 438.9 438.8 438.83 438.82 438.81 438.89 433.9 433.8 433.1 433.0 433.0 433.3 433.2 437.435.3 435.2 435.1 435.0 435.9 435.8 437.5 437.4 437.7 437.6 437.1 437.0 431 437.9 437.8 459.3 459.33 459.32 459.31 459.30 459.39 452 453 453.7 453.6 453.5 453.4 453.3 453.2 453.1 453.0 453.9 453.8 453.52 453.51 453.50 453.79 453.71 453.73 453.72 453.75 453.74 453.77 453.76 453.84 453.89 453.40 453.41 453.42 453.81 453.82 453.83 415.11 453.85 453.86 453.87 405.0 405.1 404.9 403.11 402.00 402.01 404.1 404.0 402.1 402.0 403.0 405.99 402.9 405.91 402.91 402.90 405.11 401.1 401.0 404.00 404.01 404.02 404.03 405.19 401.9 405 404.3 403.2 402 402.1 401.9 404.92 404.91 404.90 448 458.0 458.2 458.1 458.8 458.9 458.29 458.12 426.82 429.71 410.11 410.0 410.41 410.40 410.22 410.21 410.20 429.7 410.70 410.71 410.72 429.79 410.90 410.91 410.30 410.31 410.32 410.12 410.10 410.11 410.52 410.50 410.51 410.4 410.5 410.6 410.7 410.0 410.9 410.1 410.2 410.3 410.8 410.9 411.0 410.62 410.61 410.60 410.41 412.81 410.80 410.82 424.1 424.0 424.3 424.2 429.89 429.89 429.1 429.5 429.6 429.8 429.9 459.3 429.76 453.50 429.3 428.9 428.4 428.2 428.0 428.3 428.29 428.91 429.83 429.82 428.33 428.32 428.31 428.30 428.459.9 459.8 459.0 276.50 276.51 428.42 428.43 428.40 428.41 276.52 428.20 428.21 428.22 428.23 428.00 459.89 448.1 454 455 455.9 455.8 454.8 454.9 455.1 455.0 455.3 455.2 455.5 455.4 455.7 455.6 454.2 447 454.0 454.1 757.32 447.8 447.9 448.9 447.4 447.5 447.0 447.2 447.3 414.13 413.1 413.9 411.89 411.1 411 414.9 413 414.8 411.8 443.89 443.9 443.8 443.81 459.81 443.0 416.2 415.19 415.1 415.13 415.12 416.
Endocrine	Disorders Of Thyroid and other Endocrine Glands	244 244.9 244.8 244.2 255.41 255.42 255.5 255.4 255.2 255.1 255.13 259.2 243 255 253.5 259.4 255.11 242.2 240.0 241 240 240.9 241.0 242.20 242.21 241.9 241.1 253.3 704.1 255.12 255.10 255.14 246.9 246.8 246.3 246.1 246.0 246 255.3 255.8 255.6 255 252.8 252.9 252.0 252.1 252.01 252.02 252 252.08 259.52 253.4 253.6 253.1 253.0 253.2 253 253.9 253.8 242.1 242.10 242.4 242.9 242.8 242.11 242.40 242.41 376.32 242 242.31 242.30 242.91 242.40 242.80 242.81 250.32 250.20 250.30 250.22 250.42 250.40 250.02 250.00 250.10 250.12 250.82 250.80 250.90 250.92 250.50 250.52 250.72 250.60 250.70 250.62 362.05 362.01 362.07 362.06 362.0 357.2 362.03 250.7 362.02 250.8 250.9 362.04 250.2 250.3 250 250.1 250.6 250.0 250.4 250.5 259 259.3 259.50 259.9 259.8 258.8 258.92

† Categories inferred to be important for risk modulation are highlighted. Continued on next page





Integumentary	Diseases Of Skin And Subcutaneous Tissue
Respiratory	Diseases Of The Respiratory System (Distinct from Infectious)
Digestive	Diseases Of The Digestive System

† Categories inferred to be important for risk modulation are highlighted. Continued on next page





Developmental	Congenital anomalies (Non-overlap. with musculoskeletal)	<p>755.55 743.45 743.12 743.11 743.10 743.06 743.00 743.03 743.1 743.44 743.41 743.42 743.43 743.22 743.2 743.20 743.21 758.4 745.1 745.0 745.3 745.2 745.5 747.5 746.09 747 745.4 745.8 746.02 746.01 746.00 745.9 745 747.89 745.7 745.6 747.82 747.83 745.60 745.61 745.69 747.21 746.6 746.7 746.4 746.5 746.2 746.3 746.0 746.1 747.9 747.8 746.8 746.9 746.87 746.86 746.85 746.84 746.83 746.82 746.81 746.89 745.19 747.11 745.11 745.10 745.12 756.4 744.4 743.63 743.61 743.66 744.1 743.64 743.65 743.69 744.8 744.9 744.0 754.1 754.0 748.1 748.0 744.49 744.2 744.84 744.3 744.5 743.6 744.29 744.47 744.42 744.89 744.09 744.81 744.83 744.82 744.05 744.04 744.01 744.00 744.03 744.02 744.41 744.43 744.24 744.23 744.22 744.21 744.46 743.35 742.51 756.2 756.19 742.53 756.11 756.10 756.13 756.12 756.15 756.14 758.31 315.4 315.5 315.8 315.3 315.9 758 758.2 752.4 752.1 752.0 752.3 752.2 752.42 752.43 752.40 752.41 752.46 752.47 752.44 752.45 752.49 752.36 752.35 752.34 752.33 752.32 752.31 752.39 752.19 752.11 752.10 759.83 751.61 751.7 751.6 751.60 751.69 743.62 520.4 520.5 520.0 520.1 520.2 756 752.7 758.7 756.16 752.5 752.6 752.51 752.52 752.69 752.64 752.65 752.61 752.62 752.63 740 740.0 740.2 741.9 740.1 741.02 741.0 741.00 741.01 741.02 741.91 741.90 741.93 741.92 741.03 756.17 758.5 758.39 758.81 758.9 743.48 743.49 743.46 743.47 743.9 743.8 743.5 743.3 743.59 743.58 743.53 743.52 743.51 743.57 743.56 743.55 743.54 743.39 743.34 743.37 743.36 743.31 743.30 743.33 743.32 750 751.4 751.5 751.2 751.0 751.1 750.4 750.9 750.8 750.7 750.6 750.24 751.9 750.3 751.8 750.5 753.0 753.1 753.2 753.3 753.4 753.5 753.6 753.7 753.8 753.9 753.72 593.73 593.70 593.71 593.0 753.19 593.7 752.81 753.12 753.10 753.11 753.17 752.89 753 752 753.21 589 753.23 753.22 589.9 753.20 589.1 589.0 753.15 753.29 742.8 742.2 742.3 742.1 742.4 742.5 742.9 524.70 524.71 524.72 524.73 524.74 524.75 524.76 524.79 520.6 520.7 520.3 520.8 520.9 750.29 750.26 750.27 750.25 750.22 750.23 750.21 524.2 524.3 524.4 524.5 524.7 524.8 524.9 524 520 749.04 749.02 749.03 749.00 749.01 524.39 750.16 750.15 750.13 750.12 750.11 750.10 750.19 749.14 749.11 749.10 749.13 749.12 524.81 524.82 524.89 749.20 749.21 749.22 749.23 749.24 749.25 524.34 524.35 524.36 524.37 524.30 524.31 524.32 524.33 750.2 750.1 750.0 524.56 524.57 524.54 524.55 524.52 524.53 524.50 749 524.59 749.1 749.0 749.2 524.23 524.22 524.21 524.20 524.27 524.26 524.25 524.24 524.24 524.29 524.28 758.1 759.81 259.1 259.0 748.61 748.60 748 748.69 748.8 748.9 748.2 748.3 748.4 748.5 748.6 758.33 759.89 758.6 313.89 313.9 313 309.21 307.7 307.6 313.8 313.23 313.2 759.9 759.2 759.3 759.0 759.1 759.7 759.4 747.40 747.41 747.64 747.29 747.62 747.63 747.60 747.61 747.22 747.49 747.20 747.81 747.69 747.3 747.2 747.1 747.0 747.6 747.4 747.42 747.10 758.32</p>
Nutrition	Nutrition, metabolism, and development	7830,78321,7833,78340,78342,7837,7839
Health Status & Services Contact.	Vaccination, Supplementary Classification Of Factors Influencing Health Status And Contact With Health Services etc.	V01-V91

† Categories inferred to be important for risk modulation are highlighted.

---

**Algorithm 1:** ICD-9 Encoding

---

```

input : Dataset, TargetDiseaseGroup, DiseaseGroups
output: Encoding

1 Encoding ← new Dictionary();
2 for diseaseGroup ∈ DiseaseGroups do
3   Encoding[diseaseGroup][patientID] ← new List();
4   Encoding[diseaseGroup][gender] ← new List();
5   Encoding[diseaseGroup][record] ← new List();
6   Encoding[diseaseGroup][target] ← new List();
7   for record ∈ Dataset do
8     //encode Dataset into a weekly trinary sequence;
9     weeklyEncoding ← new List();
10    for weeklyDiseaseRecord ∈ record do
11      //no code recorded for the observed week;
12      if weeklyDiseaseRecord.code == NIL then
13        append "0" to weeklyEncoding;
14      if weeklyDiseaseRecord.code ∈ diseaseGroup.codes then
15        append "1" to weeklyEncoding;
16      if weeklyDiseaseRecord.code ∉ diseaseGroup.codes then
17        append "2" to weeklyEncoding;
18    target ← 1 if any weeklyDiseaseRecord.code of record ∈ TargetDiseaseGroup;
19    if target == 1 then
20      | cut weeklyEncoding up to (but not including) first occurrence of TargetDiseaseGroup member;
21      append record.patientID to Encoding[diseaseGroup][patientID];
22      append record.gender to Encoding[diseaseGroup][gender];
23      append weeklyEncoding to Encoding[diseaseGroup][record];
24      append target to Encoding[diseaseGroup][target];
25 return Encoding;

```

---

## 1. Pipeline Optimization

### 1.1. Input Data Format

To encode the ICD-9 codes, 17 Disease Groups of codes are used to transform the raw health records into a format suitable for PFSA. As described in *Algorithm 1*, for each patient, the list of ICD-9 codes is encoded into a weekly array of three-symbol alphabet digits with respect to selected disease group, for each week: "0" - no disease "1" - disease from the selected group, "2" - other disease.

Once the trinary encodings are ready, the PFSA pairs are fit for each of the disease groups, on positive (treatment) and negative (control) sets using genESeSS algorithm<sup>2</sup> (See Section 11), as described in *Algorithm 2*. The PFSA pairs are then used to obtain the loglikelihood scores of belonging to a PFSA modeling the positive and the control cohorts accordingly for each of the encodings of a patient record. As a result, we yield the difference between positive and control loglikelihoods for each disease group of each patient. The positive value of difference means that with respect to a given disease group, a certain patient is more likely to be a positive one. Conversely, the negative value of difference signifies that a patient is more likely to be from the control group. These features, as well as their aggregations and the aggregations of the ternary encoding arrays, are used as the features for the final LightGBM gradient boosting classifier.

### 1.2. Algorithms

The key data processing approach is outlined in Algorithm 1. The remaining steps of the approach are sketched in Algorithm 2. Fig. 8 shows the overall schema, including the breakdown of a database into a test set, and two training sets: one for training the HMM models, and one for training the boosting classifier.

---

**Algorithm 2:** Prediction Pipeline Training

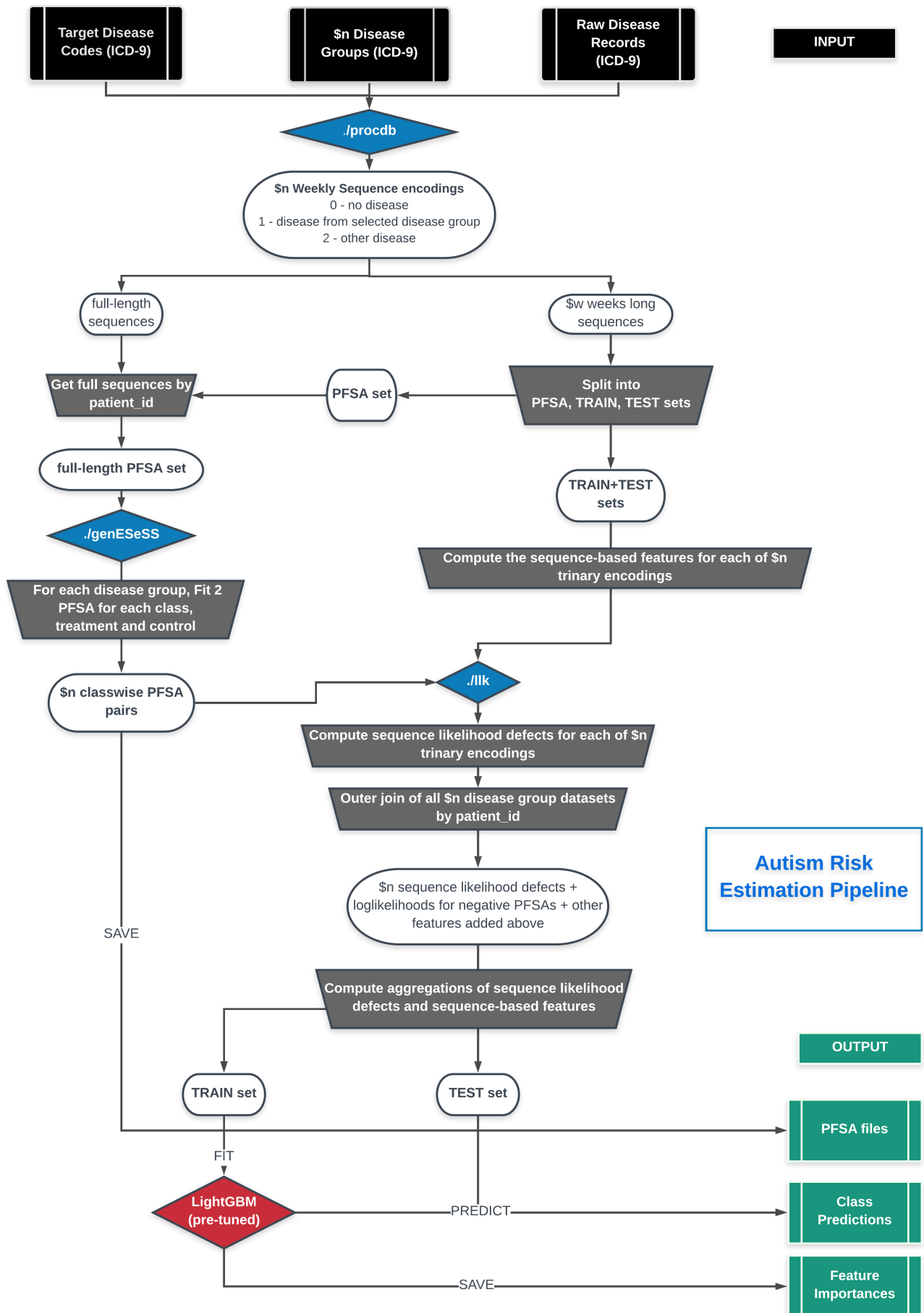
---

**input** : Encoding, DiseaseGroups, SequenceFeatures, hyperparameters  
**output:** Predictions, FeatureImportances

```

1 DiseaseDatasets ← new Dictionary();
2 for Dataset, DiseaseGroup ∈ zip(Encoding, DiseaseGroups) do
3     PFSAsset, LLset ← TrainTestSplit(Dataset, w.r.t = "target");
4     df ← new Dataframe();
5     df[patientID] ← LLset[patientID];
6     df[target] ← LLset[target];
7     //Generate 2 PFSAs for each class;
8     PositivePFSAsset ← PFSAsset[PFSAsset.target == 1];
9     NegativePFSAsset ← PFSAsset[PFSAsset.target == 0];
10    PosPFSA ← genESeSS(PositivePFSAsset);
11    NegPFSA ← genESeSS(NegativePFSAsset);
12    //For each record, compute loglikelihoods of being generated by either of 2 PFSAs generated above;
13    PosLLK ← llk(LLset, PosPFSA);
14    NegLLK ← llk(LLset, NegPFSA);
15    //Compute sequence likelihood defect;
16    df[DiseaseGroup] ← pairwise(PosLLK - NegLLK);
17    df[DiseaseGroup + '_abs_neg'] ← NegLLK;
18    for SequenceFeature ∈ SequenceFeatures do
19        df[DiseaseGroup + '_' + SequenceFeature] ← [ComputeSequenceFeature(SequenceFeature,
20                                              seq) for each seq ∈ LLset['record']];
20    DiseaseDatasets[DiseaseGroup] ← df;
21 Dataset ← outerjoin(DiseaseDatasets.values, on = 'patientID');
22 Aggregate all features in Dataset where feature_name ∈ DiseaseGroups (mean, std. deviation, range);
23 Aggregate all features in Dataset where feature name minus '_abs_neg' ∈ DiseaseGroups (mean, std.
    deviation, range);
24 Aggregate all sequence features in Dataset (mean, std. deviation, range, max);
25 TrainSet, TestSet ← TrainTestSplit(Dataset, w.r.t = "target");
26 LGBM ← new LightGBM(hyperparameters);
27 LGBM.fit(TrainSet);
28 Predictions ← LGBM.predict(TestSet);
29 return Predictions, LGBM.feature_importances;
```

---



SI-Fig. 8: Pipeline schema: How the data set is split into test sets and two training sets: one for inferring HMM models, and one for training the boosting classifier. The two ket algorithms here are `genESeSS`<sup>2</sup> and the `llk` which does the sequence likelihood computation described in Section 12

## 2. Example Run with Released Application



SI-Fig. 9: Screen capture of the page on pypi.org hosting the released application Link: <http://pypi.org/ehrzero>

```
[1]: from ehrzero import ehrzero as ehr
      import warnings
      warnings.filterwarnings("ignore")

[2]: source = 'test_free.dat'
      outfile = 'out.dat'
      first_weeks = [200, 100] # number of first weeks of the observations to consider
      risks = ehr.predict_with_confidence(source,
                                           outfile,
                                           separator = ',',
                                           delimiter = ' ',
                                           n_first_weeks = first_weeks)

[3]: risks
```

	patient_id	week	risk	relative_risk	confidence
0	AAbby	200	0.000174	0.028200	0.920977
0	AAbby	100	0.000135	0.021954	0.954741
1	ALorax	200	0.000101	0.016416	0.989583
1	ALorax	100	0.000099	0.016071	0.986710

SI-Fig. 10: Python code prediction example

### 2.1. Prerequisites & Installation

The minimum prerequisites for running ehrzero are the following:

1. A x64 system running any flavor of Linux.
2. A working python 3.x installation
3. scikit-learn, version = 0.20.0

Installation:

```
pip3 install ehrzero --user
```

## 2.2. EHR data format

Diagnostic data stored in text file, one line per patient as follows: patient id, gender, and list of space-separated, comma-delineated diagnosis records, all separated by spaces. Each diagnosis record consists of the week since the start of the observation, followed by a comma, and the ICD-9 code of the diagnosis.

Example of a patient line:

```
Lorax,M 5,277.03 10,611.79 18,057.8 58,157.8 78,057.8 108,057.8 128,057.8 148,057.8
```

## 2.3. Sample Python code risk estimation

Once the patient diagnostic data is in the required format, for function `predict_with_confidence` we specify the filepath of the data and the list of the cutoffs for the first weeks since the start of observations for the data we want to analyze. We also specify the separator and delimiter for the patients within file (space and comma are default values, but can be changed for user convenience).

The `predict_with_confidence` function returns the predicted risk of autism for every patient in the input file with all the specified numbers of first weeks to consider.

## 2.4. Sample Python script risk estimation

The script version is similar to the one mentioned before.

Once `ehrzero` package is installed, locate its directory and go to `texttt../ehrzero/example`. Select one of the `".dx"` or `".dat"` files in `/ehrzero/example/tests` as input and run the following command as an example:

```
python zero.py -data tests/ZEROexample.dat -outfile predictions.csv -nweeks 100 200  
300 -Verbose 1
```

```
(base) [onishchenko@midway2-login1 example]$ cat tests/ZERO_example.dat  
M:44 380.10:101 381.81:11 084.6  
M:9 380.10:104 381.81:11 084.6  
M:99 380.10:104 381.81:11 084.6:98 380.11  
M:9 380.10:104 381.71:11 084.6  
M:9 390.11:4 390.11:4 381.71:11 084.6  
(base) [onishchenko@midway2-login1 example]$ python zero.py -data tests/ZERO_example.dat -outfile predictions.csv -n_weeks 100 200 300 -Verbose 1  
patient_id week risk relative_risk confidence  
A000000001 100 0.001703 0.098002 68.54  
A000000001 200 0.001834 0.105517 72.43  
A000000001 300 0.001834 0.105517 72.43  
A000000002 100 0.002030 0.116816 60.94  
A000000002 200 0.001426 0.002033 80.01  
A000000002 300 0.001426 0.002033 80.01  
A000000003 100 0.001703 0.098002 68.54  
A000000003 200 0.001705 0.098170 74.53  
A000000003 300 0.001853 0.106625 72.18  
A000000004 100 0.000512 0.029449 94.86  
A000000004 200 0.001450 0.083436 79.53  
A000000004 300 0.001450 0.083436 79.53  
A000000005 100 0.000658 0.037868 91.73  
A000000005 200 0.000658 0.037868 95.21  
A000000005 300 0.000658 0.037868 95.21  
(base) [onishchenko@midway2-login1 example]$
```

SI-Fig. 11: Python script prediction example

## 3. Comparison With State of the Art Off-the-shelf ML Algorithms

Off the shelf algorithms with little or no pre-processing, *i.e.*, using the diagnostic codes themselves are time-stamped categorical features failed to produce clinically relevant performance (See Fig. 3). Classifiers such as random forests<sup>3</sup>, and gradient boosters<sup>4</sup> might be penalized due to their inability to take into account long-range temporal information. Since the number of diagnostic codes available per patient is small, recurrent neural network implementations such as LSTM<sup>5</sup> might be suffering from the data sparsity in training. It is possible that the performance of the competing approaches might be improved with extensive tuning or clever feature-engineering.

## 4. Comparison With Pipeline Variations, Feature Subsets and Neural Net Post-processing

In addition to the naive baseline approaches, we also evaluated the performance achievable with LSTMs (denoted as LSTM<sub>B</sub> in Fig. 3) that use identical preprocessing as our pipeline, *i.e.*, representation of diagnostic histories as trinary sequences in 18 categories for each patient, and achieved  $\sim 80\%$  AUC at 150 weeks for males in the Truven database (compared to  $> 85\%$  for our approach). However, the performances drop significantly when the number of positive samples is reduced, yielding an AUC of 66% on the UCM dataset for males, 60% for females on the Truven dataset, and a worse-than-random 40% on the UCM dataset respectively (See Fig. 3).

Much better results were obtained when we compared our optimized pipeline to pipelines that use only a subset of our features: namely, the ones that use only features derived from sequence statistics and exclude the ones derived from learning PFSAs (recall that PFSAs are special HMMs we learn using our novel algorithms) from the disease categories as described in Methods in the main text, or using only the PFSA-based SLD features, or using simply the density of diagnostic codes (See Fig. 5, panel D). In all these cases we analyzed, our pipeline has a clearly demonstrable advantage (See Fig. 5, panel D) that is stable across databases, under reductions in sample sizes, and in balanced resampling experiments (See Fig. 5, panel C).

While it is difficult to explain the exact source of a modeling framework's performance, and even more difficult to explain non-performance, we can point to the following advantages that our approach has over existing techniques:

1. **Purely Classification Algorithms With No Pre-processing Do not Do well.** Pure classifiers such as random forests, gradient boosters, etc. are not time series modeling frameworks, and might not capture stochastic temporal patterns well. While features are not certainly assumed to be independent in these algorithms, it is problematic to learn patterns that do not appear at fixed time points in the diagnostic history.
2. **Lower Sample Complexity Compared to Deep Learning Frameworks.** Compared to LSTMs and RNNs, we are able to capture stochastic behavior with more compact models, which results in better sample complexity. In other words, if we have less data, our models do better, because we estimate fewer parameters.
3. **Designed Bottom-up for Learning Stochastic Processes.** It is easily demonstrated that LSTMs and RNNs, while good models of complicated time series in many cases, do not work well for data that are generated by stochastic processes, *i.e.* are sample paths of a hidden process.
4. **We May Have Missed Some Clever Transformation.** It is possible that extensive tuning or feature selection with LSTMs, RNNs or CNNs or some combination thereof, can replicate our performance, or even do better. There will always be that possibility, notwithstanding how much effort we put in to evaluate competing techniques. The authors welcome *future work in this direction that surpasses our performance reported here; this is only going to help the patients which is what matters.*

### 4.1. Feature Subset Evaluations & Code Density As A Feature

With regards to Fig. 5, panel D, we note that the PFSA based features by themselves are comparable to those engineered manually from sequence statistics (the latter include features such as the proportion of codes in a patient's history corresponding to specific disease categories, mean and variance of adjacent empty weeks *etc.*, see main text Table III in the main text for details), but the combined runs produce significantly superior results. Also, it is interesting to note that simply using the density of diagnostic codes in a child's history is quite predictive of future ASD diagnosis, with the AUC from using just the density of codes as a feature rising to over 75% in the Truven database at 150 weeks. However, it does not have stable predictive performance across databases, and is also the least performing predictor. We did not include code density in our combined feature set, since it has no effect once the rest of the features are combined.

## 5. Threshold Selection on ROC Curve

Once the ROC curve has been computed, we must choose a decision threshold to trade-off true positive rate and false positive rate. In situations where the number of negatives vastly outnumber the number of positives (which

is the case in our problem), it is better to base this trade-off on a measure that is independent of the number of true negatives. The two popular measures considered in the literature are accuracy and the F1-score:

$$\text{accuracy} = \frac{t_p + t_n}{t_p + f_p + f_n + t_n} \quad (1)$$

$$\text{F1} = \frac{2t_p}{2t_p + f_p + f_n} \quad (2)$$

The F1-score is the same as accuracy where the number of true negatives is the same as the number of true positives, thus partially correcting for the class imbalance.

The selection of the threshold may also be dictated by the current practice of ensuring high specificities in screening tests. Thus, the most relevant clinically operating point is probably the one corresponding to 95% specificity, which is highlighted in Fig. 2C in the main text.

## 6. Note on Receiver Operating Characteristics (ROC) and Precision-recall Curves

The ROC curve is a plot between the False Positive rate (TPR) and the True Positive Rate (TPR), and the area under the ROC curve (AUC) is often used as a measure of classifier performance. For the sake of completeness, we introduce the relevant definitions:

In the following  $P$  denotes the total number of positive samples (number of patients who are eventually diagnosed), and  $N$  denotes the total number of negative samples (number of patients in the control group).

**Definition 1.** *True positive rate, true negative rate, false positive rate, positive predictive value (PPV), and prevalence ( $\rho$ ) are defined as:*

$$\text{TPR} = \frac{t_p}{P} = \frac{t_p}{t_p + f_n} \quad (3)$$

$$\text{TNR} = \frac{t_n}{N} = \frac{t_n}{t_n + f_p} \quad (4)$$

$$\text{FPR} = 1 - \text{TNR} \quad (5)$$

$$\text{PPV} = \frac{t_p}{t_p + f_p} \quad (6)$$

$$\rho = \frac{P}{N + P} \quad (7)$$

where as before  $t_p, t_n, f_p, f_n$  are true positives, true negatives, false positives, and false negatives respectively.

Note that TPR is also referred to as **recall** or **sensitivity**, and PPV is also referred to as **precision**. True negative rate is also known as **specificity**.

A **precision-recall curve**, or a PPV-sensitivity curve is a plot between PPV and TPR.

Denoting sensitivity by  $s$ , and specificity by  $c$ , it follows that:

$$\text{PPV} = \frac{t_p/P}{t_p/P + (f_p/N)(N/P)} = \frac{\text{TPR}}{\text{TPR} + ((N - t_n)/N)(N/P)} \quad (8)$$

$$\Rightarrow \text{PPV} = \frac{s}{s + (1 - c)(\frac{1}{\rho} - 1)} \quad (9)$$

Thus, we note that for a fixed specificity and sensitivity, the PPV depends on prevalence. Indeed, it is clear from the above argument that PPV decreases with decreasing prevalence, and vice versa, if specificity and sensitivity are held constant. Also, if prevalence is limited to 2%, and specificity is held at 95%, then the maximum PPV is limited to:

$$\text{PPV} = s/(s + 2.45) \leq 1/3.45 \sim 29\% \quad (10)$$

This shows that for ASD screening, we can hope for a maximum PPV of ~29% at 95% specificity, if the prevalence is stable at around 2%.

Compare this with the PPV of 15.8% (M) and 18.8% (F) that we achieve at 51.8% sensitivity, where the specificity is held at 95% in Fig. 2C in the main text. Note here that M-Chat/F with follow-up has a PPV of 14.6% as reported by the recent CHOP study<sup>1</sup>.

## 7. Effect of Class Imbalance

ROC curves are generally assumed to be robust to class imbalance. Note that if we assume that patient outcomes are independent (which is well-justified in the case of a non-communicable condition, particularly in large databases), then  $t_p$  should scale linearly with the total number of positives  $P$ , implying:

$$\text{TPR} = \frac{t_p}{P} = \frac{t'_p}{P'} \quad (11)$$

implying that with different sizes of the set of positive samples (or negative samples), the ROC curve remains unchanged. In particular, note that even if the prevalence is very small (say 0.01%), we cannot cheat to boost the AUC by labeling all predictions as negative, or stating that risk is always zero: in that case, our  $P$  is very small, but our  $t_p = 0$  strictly, implying that our  $\text{TPR} = 0$ , thus leading to a zero AUC. We can cheat to boost the accuracy (See the previous section), but not the AUC.

Note that while relative class sizes or imbalance does not affect the ROC (under the assumption that true positives and true negatives scale with the number of positives and negatives), very small absolute sample sizes might still result in poor performance of the model.

We do have significant class imbalance in our datasets. This arises naturally from the low prevalence rate of ASD (small in the sense of comparison of sizes of the control and the positive cohorts). Thus, we validated if the performance of our predictive pipeline remains unchanged by replacing the full control cohort with a random sample of size equal to that of the positive cohort. The results, shown in Fig. 5C, illustrate that class imbalance has no appreciable effect on our pipeline, as far as the AUC metric is considered.

The precision-recall curves do get affected by class imbalance, or the prevalence, as shown by Eq (9). However, in diagnostic analysis, they are important since we are generally less interested in the number of true negatives; the ratio of false positives to the total number of positive recommendations by the algorithm is much more relevant, *i.e.*, the PPV or the precision.

We have used this to our advantage. Note that since the PPV is affected by prevalence, a stratification of the total population with different prevalence in each sub-population suggests the possibility of a conditional choice of the operating point, thus boosting the overall PPV. We describe this approach in the sequel, in Section 9.1. First, we establish that our pipeline does not suffer from some important pitfalls arising in the workflows associated with ASD diagnosis, and how the diagnostic codes in Electronic Health Records (EHR) are generated.

## 8. Note on ASD Clinical Diagnosis & Uncertainty of EHR Record

With no precise laboratory test for ASD, most families experience the following sequence of events<sup>6-8</sup>: 1) routine screening at 18 and 24 months of age identifies high risk, and is followed by 2) a diagnostic evaluation. The American Academy of Pediatrics (AAP) recommends screening all children for symptoms of ASD at 18 and 24 months of age in their primary care visits<sup>9,10</sup>. However, results of a screening test are not diagnostic (*and hence do not produce an EHR diagnostic code*); they help the primary care provider identify children who are at risk for a diagnosis of ASD and require additional evaluation. The M-CHAT/F is the most studied and widely used tool for screening toddlers for ASD<sup>8,11</sup>.

Unfortunately, children with milder symptoms are harder to screen for. The AAP warns that children with milder symptoms and/or average or above-average intelligence may not be identified with symptoms until school age, when differences in social language or personal rigidities affect function<sup>8</sup>.

### 8.1. Diagnostic Evaluations

Once a child is determined to be at risk for a diagnosis of ASD, either by screening or surveillance, a timely referral is needed for clinical diagnostic evaluation<sup>7</sup>, which will, on positive identification, assign a clinical diagnosis, and produce an EHR record.

The history of symptoms of ASD presentation in individual patients may be elucidated by questionnaires such as the Social Communication Questionnaire (SCQ), or Social Responsiveness Scale (SRS), or the Autism Diagnostic Interview-Revised (ADI-R)<sup>8</sup>. These questionnaires alone are insufficient for making a clinical diagnosis, but provide a structured approach to elicit symptoms. Validated observation tools used to provide structured data to

confirm a clinical diagnosis include the Autism Diagnostic Observation Schedule, Second Edition (ADOS-2)<sup>12</sup> and the Childhood Autism Rating Scale, Second Edition (CARS-2)<sup>13</sup>. Current guidance from the American Academy of Pediatrics<sup>8</sup> notes that no single observation tool is universally appropriate, and that such tools are meant to support the application of the diagnostic criteria informed by history and other data.

At present, the Autism Diagnostic Interview-Revised (ADI-R) and Autism Diagnostic Observation Schedule (ADOS) are considered the “gold standard” tools to enable the diagnosis of ASD<sup>14</sup>. The true “gold standard” classification and diagnosis of autism is historically taken to be a multi-disciplinary team (MDT) clinical assessment, including use of the ADOS and ADI-R, as well as other assessments with consensus clinical judgment<sup>14</sup>. The MDT clinical diagnosis correct classification rate for ASD is approximately 80.8%. Thus, any individual tool that correctly classifies ASD at a rate of 80 % or over could be considered to be just as accurate as the “gold standard”<sup>14</sup>. With ADOS-2 and associated tools verifiably reaching this classification rate, the current APA guidance suggests that individual general pediatricians might hand out initial diagnoses if they are familiar with the relevant DSM diagnostic criteria. This simultaneously raises the prevalence, and the possibility that some diagnostic codes pertaining to ASD in medical history databases could be arising from less restrictive workflows, and thus might carry more uncertainty.

In our study, we checked if restricting the treatment cohort to children with at least two distinct ASD diagnostic codes in their medical histories instead of one (which significantly reduces the possibility of erroneous coding) changes the performance of the algorithm. The results shown in Fig. 5B illustrate that we have very little change in out-of-sample predictive performance, thus alleviating this concern.

### *8.2. Change In Diagnostic Criteria for ASD, Inclusion of PDD, Asperger, and Disambiguation From Unrelated Psychiatric Phenotypes*

The DSM-5 established a single category of ASD to replace the subtypes of autistic disorder, Asperger syndrome, and pervasive developmental disorder not otherwise specified in the Diagnostic and Statistical Manual of Mental Disorders, Fourth Edition, Text Revision (DSM-IV-TR)<sup>8</sup>. This justifies our use of diagnostic codes from ICD9 299.X as specification of an ASD diagnosis, and use of GEMS mapping to 299.X for ICD10 codes when we encounter them. Future renditions of our pipeline will use purely ICD-10 specification, which does not change the algorithm, but merely how we input data into it.

It is interesting to note that we would be actually unable to discriminate between those phenotypes effectively for high predictability even if we wanted: in our initial efforts, we found it is very difficult to design a high performing pipeline that recognizes these sub-types separately.

The question then arises as to how well we can discriminate between ASD and other unrelated psychiatric phenotypes. Does our pipeline pick up on any psychiatric conditions, or is it specific to ASD? We directly evaluated this, by restricting the test control cohort to patients with at least one psychiatric code other than ASD. We get very high discrimination reaching AUCs over 90% at 100-125 weeks of age, which establishes that our pipeline is indeed largely specific to ASD.

### *8.3. Performance Comparison With M-CHAT/F*

The M-CHAT/F is the most studied and widely used tool for screening toddlers for ASD<sup>8,11</sup>.

Guthrie *et al.*<sup>1</sup> from the Children’s Hospital of Philadelphia (CHOP) demonstrate that when applied as a universal screening tool, M-CHAT/F has a sensitivity of 38.8%, specificity of 94.9% and PPV of 14.6%. This work is the only large-scale study of M-CHAT/F (n=20,375) we are aware of with sufficient follow-up after the age of four years to provide a reasonable degree of confidence in the sensitivity of M-CHAT/F.

Comparing the performance metrics achieved at different age groups across data sets and sexes for our pipeline (See main text Table IV in the main text), we conclude that our approach produces a strictly superior PPV (exceeding M-CHAT/F PPV by at 14% (14.1-33.6%) when sensitivity and specificity are held at comparable values around the age of 26 months ( $\approx$  112 weeks). We cannot compare at other operating points due to a lack of M-CHAT/F performance characterization anywhere else.

Apart from standalone performance, our proposed approach has several key advantages: it is clearly immune to parental educational level, and language barriers. Since access to insurance and medical records do get impacted by socio-economic variables, there is the possibility of some indirect impact from the demographic

makeup of the training datasets. But overall, diagnostic histories are free from biases that have historically plagued questionnaire-based screens<sup>8</sup>. Additionally, while M-CHAT/F is relatively easy and quick to administer, the issue of time and resource commitment cannot be ignored<sup>8</sup>. These factors conspire to produce reduced coverage, which in turn casts doubt upon the necessity of universal screening programs despite clear guidance on the contrary from the AAP<sup>1</sup>.

Additionally, being functionally independent of the M-CHAT/F, we can take advantage of any population stratification induced by the M-CHAT/F results to significantly boost combined screening performance.

## 9. Improving Wait-times For Diagnostic Evaluations by Reducing False Positives in Routine Screening

While children with ASD can be diagnosed as toddlers<sup>15,16</sup> (developmental concerns may show up before the first birthday<sup>17,18</sup>), the mean age of diagnosis is over 4 years<sup>19</sup>. Since a clinical diagnosis of ASD requires the multi-step process described in the previous section, this delay mainly arises from extended wait-times and queues, which ultimately delays entry into early intervention (EI) programs. While time-consuming evaluations<sup>20</sup>, cost of care<sup>21</sup>, lack of providers<sup>22</sup>, lack of comfort in diagnosing by primary care providers<sup>22</sup>, and other challenges, are all responsible to varying degrees that culminate in these delays<sup>6</sup>, one rather obvious source is the limited PPV of screening tests that are available today. With the PPV of M-CHAT/F being around 14.6%, over 85 out of 100 people flagged for diagnostic evaluation are false positives, leading to wait times that currently range from 3 months to 1 year. To make matters worse, access to care and resources are sparse except near urban centers. For example, only 7% of developmental pediatricians practice in rural areas, and some states do not even have a developmental pediatrician<sup>6,23</sup>.

A key contribution of this work is to be able to significantly reduce the number of false positives without sacrificing specificity, and thus significantly improving wait-times and patient outcomes.

### 9.1. 4D Decision Optimization Using M-CHAT/F Population Stratification To Boost PPV

Assume that there are  $m$  sub-populations such that: the total number of positives and negatives, and the prevalences in each sub-population are given by  $P_i, N_i$  and  $\rho_i$  respectively, with  $i \in \{1, \dots, m\}$ . Let  $\beta_i$  be the relative size of the sub-populations. Thus, we have:

$$P = \sum_i P_i \quad (12)$$

$$N = \sum_i N_i \quad (13)$$

$$\beta_i = \frac{N_i + P_i}{N + P} \quad (14)$$

$$\rho_i = \frac{P_i}{N_i + P_i} = \frac{P_i}{\beta_i(N + P)} \quad (15)$$

Therefore, denoting the sensitivity and specificity of the sub-populations as  $s_i$  and  $c_i$  respectively, we have:

$$s = t_p/P = \frac{\sum_i t_p|_i}{P} = \frac{\sum_i (t_p|_i/P_i) \times (\beta_i \rho_i (P + N))}{P} = \sum_i s_i \beta_i \frac{\rho_i}{\rho} \quad (16)$$

Thus, we end up with:

$$s = \sum_{i=1}^m s_i \gamma_i \quad (17a)$$

$$c = \sum_{i=1}^m c_i \gamma'_i \quad (17b)$$

$$PPV = \frac{s}{s + (1 - c)(\frac{1}{\rho} - 1)} \quad (17c)$$

where we have denoted:

$$\gamma_i = \beta_i \frac{\rho_i}{\rho}, \text{ and } \gamma'_i = \beta_i \frac{1 - \rho_i}{1 - \rho} \quad (17d)$$

Now, using Table 2, we can compute the values for  $\gamma_i, \gamma'_i$ , as shown below.

Using the prevalence and stratification parameters calculated from the CHOP study (See main text Table 3<sup>1</sup>), we can compute a conditional choice of sensitivity and specificity for our tool, in each sub-population to ultimately yield an overall performance significantly superior to M-CHAT/F. We carry out a four-dimensional search at the age the CHOP population stratification is reported (26 months or 112 weeks approximately) to identify the feasible region with  $PPV > 14.6\%$ , or sensitivity  $> 38.8\%$  while keeping specificity  $> 94.9\%$  where each of these dimensions represent the independent choice of sensitivity in the corresponding sub-population. For each set of 4 choices, the corresponding specificities are read-off from our computed ROC curve, and then the overall sensitivity, specificity and PPV are calculated using Eq. (17). The results are shown in Fig. 4, where we include the computations at 75 weeks, 125 weeks, and 150 weeks, with the same population stratification (although understandably the stratification will deviate from the values obtained at 26 months for those other ages).

An important assumption here is that the two tests are independent. Since M-CHAT/F is based on the detection of behavioral signals of developmental delay associated with autism via questionnaires completed by the primary care-givers, while our pipeline is based on physical comorbidities, independence is reasonable. Hence, we can simulate the application of the pipeline to each sub-population, and compute the overall performance quantities using a pre-computed ROC curve. Here we use the curve corresponding to the age in weeks, but average the male and female ROC curves, which are close as shown in Fig. 2 in the main text. The male-female averaging is necessary since the results from the CHOP study does not report sex stratified data.

We show the feasible region obtained by this computation in Fig. 4 of this document, and in main text Fig. 4 of the main text. Particularly, note that we get a PPV close to or higher than 30% at the high precision (HP) operating point, or a sensitivity above 55% for the high recall (HR) operating point, when we restrict specificities to above 95%.

It is important to note that Eq. (17) and hence the results are dependent on the population prevalence  $\rho$ . We report the dependence of the solution to the 4D optimization for population prevalence between 1.7% (CDC estimate<sup>8</sup>), and 2.23% (CHOP estimate<sup>1</sup>). In particular, it is illuminating to compare these results directly with M-CHAT/F performance, as shown in Fig. 4, panels B and C in the main text. In panel C, we show that for any stable population prevalence between 1.7% and 2.24%, we can achieve nearly double the PPV without losing sensitivity, or increase the sensitivity by about 50% without sacrificing PPV, while holding not letting the specificity to drop below 94%.

## 10. Generating PFSA Models From Set of Input Streams with Variable Input Lengths

Our PFSA reconstruction algorithm<sup>2</sup> is distinct from standard HMM learning. We do not need to pre-specify structures, or the number of states in the algorithm, and all model parameters are inferred directly from data. Additionally, we can operate either with 1) a single input stream, or 2) a set of input streams of possibly varying lengths which are assumed to be different and independent sample paths from the unknown stochastic generator we are trying to infer. At an intuitive level, we use the input data to infer the length of histories one must remember to estimate the current state, and predict futures for the process being modeled. Thus, we do not step through the symbol streams with a pre-specified model structure, and avoid the need to have equal-length inputs. More details of the algorithm are provided in the next section.

The ability to model a set of input streams of varying lengths is particularly important, since medical histories of different patients are typically of different lengths.

## 11. Probabilistic Finite State Automata Inference

### 11.1. Probabilistic Finite-State Automaton

Let  $\Sigma$  be a finite alphabet of symbols with size  $|\Sigma|$ . The set of sequences of length  $d$  over  $\Sigma$  is denoted by  $\Sigma^d$ . The set of finite but unbounded sequences over  $\Sigma$  is denoted by  $\Sigma^*$ , the Kleene star operation<sup>24</sup>, i.e.  $\Sigma^* = \bigcup_{d=0}^{\infty} \Sigma^d$ . We use lower case Greek, for example  $\sigma$  or  $\tau$ , for symbols in  $\Sigma$ , and lower case Latin, for example  $x$  or  $y$ , for sequences of symbols, i.e.  $x = \sigma_1 \sigma_2 \dots \sigma_n$ . We use  $|x|$  to denote the length of  $x$ . The empty sequence is denoted by  $\lambda$ .

We denote the set of strictly infinite sequences over  $\Sigma$  by  $\Sigma^\omega$ , and the set of strictly infinite sequences having  $x$  as prefix by  $x\Sigma^\omega$ . Let  $\mathcal{S} = \{x\Sigma^\omega : x \in \Sigma^*\} \cup \{\emptyset\}$ , we can verify that  $\mathcal{S}$  is a semiring<sup>25</sup> over  $\Sigma^\omega$ . We use  $\mathcal{F}$  to denote the sigma algebra generated by  $\mathcal{S}$ .

**Definition 2** (Stochastic Process over  $\Sigma$ ). A stochastic process over a finite alphabet  $\Sigma$  is a collection of  $\Sigma$ -valued random variables  $\{X_t\}_{t \in \mathbb{N}}$  indexed by positive integers<sup>26</sup>.

We are specifically interested in processes in which the  $X_i$ 's are not necessarily independently distributed.

**Definition 3** (Sequence-Induced Measure and Derivative). For a process  $\mathcal{P}$ , let  $Pr_{\mathcal{P}}(x)$  or simply  $Pr(x)$  denote the probability  $\mathcal{P}$  producing a sample path prefixed by  $x$ . The measure  $\mu_x$  induced by a sequence  $x \in \Sigma^*$  is the extension<sup>25</sup> to  $\mathcal{F}$  of the premeasure defined on the semiring  $\mathcal{S}$  given by

$$\forall x, y \in \Sigma^*, \mu_x(y\Sigma^\omega) \triangleq \frac{Pr(xy)}{Pr(x)}, \text{ if } Pr(x) > 0 \quad (18)$$

For any  $d \in \mathbb{N}$ , the  $d$ -th order derivative of a sequence  $x$ , written as  $\phi_x^d$ , is defined to be the marginal distribution of  $\mu_x$  on  $\Sigma^d$ , with the entry indexed by  $y$  denoted by  $\phi_x^d(y)$ . The first-order derivative is called the **symbolic derivative** and is denoted by  $\phi_x$  for short.

**Definition 4** (Probabilistic Nerode Equivalence and Causal States<sup>27</sup>). For any pair of sequences  $x, y \in \Sigma^*$ ,  $x$  is equivalent to  $y$ , written as  $x \sim y$ , if and only if either  $Pr(x) = Pr(y) = 0$ , or  $\mu_x = \mu_y$ . The equivalence class of a sequence  $x$  is denoted by  $[x]$  and is called a **causal state**<sup>28</sup>. The cardinality of the set of causal states is called the **probabilistic Nerode index**, or the Nerode index for simplicity.

We can see from the definition that causal states captures how the history of a process influences its future. Since the probabilistic Nerode equivalence is right invariant, it gives rise naturally to a automaton structure introduced below.

**Definition 5** (Probabilistic Finite-State Automaton (PFSA)). A PFSA  $G$  is defined by a quadruple  $(Q, \Sigma, \delta, \tilde{\pi})$ , where  $Q$  is a finite set,  $\Sigma$  is a finite alphabet,  $\delta : Q \times \Sigma \rightarrow \Sigma$  is called the transition map, and  $\tilde{\pi} : Q \rightarrow \mathbf{P}_\Sigma$ , where  $\mathbf{P}_\Sigma$  is the space of probability distributions over  $\Sigma$ , is called the transition probability. The entry of  $\tilde{\pi}(q)$  indexed by  $\sigma$  is denoted by  $\tilde{\pi}(q, \sigma)$ .

**Definition 6** (Transition and Observation Matrices). The transition matrix  $\Pi$  is the  $|Q| \times |Q|$  matrix with the entry indexed by  $q, q'$ , written as  $\pi_{q,q'}$ , satisfying

$$\pi_{q,q'} \triangleq \sum_{\{\sigma \in \Sigma | \delta(q, \sigma) = q'\}} \tilde{\pi}(q, \sigma) \quad (19)$$

and the observation matrix  $\tilde{\Pi}$  is a  $|Q| \times |\Sigma|$  matrix with the entry indexed by  $q, \sigma$  equaling  $\tilde{\pi}(q, \sigma)$ .

We note that both  $\Pi$  and  $\tilde{\Pi}$  are stochastic, i.e. non-negative with rows summing up to 1.

**Definition 7** (Extension of  $\delta$  and  $\tilde{\pi}$  to  $\Sigma^*$ ). For any  $x = \sigma_1 \dots \sigma_k$ ,  $\delta(q, x)$  is defined recursively by

$$\delta(q, x) \triangleq \delta(\delta(q, \sigma_1 \dots \sigma_{k-1}), \sigma_k) \quad (20)$$

with  $\delta(q, \lambda) = q$ , and  $\tilde{\pi}(q, x)$  is defined recursively by

$$\tilde{\pi}(q, x) \triangleq \prod_{i=1}^k \tilde{\pi}(\delta(q, \sigma_1 \dots \sigma_{i-1}), \sigma_i) \quad (21)$$

with  $\tilde{\pi}(q, \lambda) = 1$ .

**Definition 8** (Strongly Connected PFSA). We say a PFSA is strongly connected if the underlying directed graph is strongly connected<sup>29</sup>. More precisely, a PFSA  $G = (Q, \Sigma, \delta, \tilde{\pi})$  is strongly connected if for any pair of distinct states  $q$  and  $q' \in Q$ , there is an  $x \in \Sigma^*$  such that  $\delta(q, x) = q'$ .

We assume all PFSA in the discussions in the sequel are strongly connected if not specified otherwise. For strongly connected PFSA  $G$ , there is a unique probability distribution over  $Q$  that satisfies  $\mathbf{v}^T \Pi = \mathbf{v}^T$ . This is the **stationary distribution**<sup>30,31</sup> of  $G$  and is denoted as  $\varphi_G$ , or  $\varphi$  if  $G$  is understood.

**Definition 9** ( $\Gamma$ -Expression). We can encode the information contained in  $\delta$  and  $\tilde{\pi}$  by a set of  $|Q| \times |Q|$  matrices  $\Gamma = \{\Gamma_\sigma | \sigma \in \Sigma\}$ , where

$$\Gamma_\sigma|_{q,q'} \triangleq \begin{cases} \tilde{\pi}(q, \sigma) & \text{if } \delta(q, \sigma) = q', \\ 0 & \text{if otherwise.} \end{cases} \quad (22)$$

$\Gamma_\sigma$  is called **event-specific transition matrix**, with the event being that  $\sigma$  is current the output.  $\Gamma_\sigma$  can also be extended to arbitrary  $x \in \Sigma^*$  by defining  $\Gamma_x = \prod_{i=1}^k \Gamma_{\sigma_i}$  with  $\Gamma_\lambda = I$ .

**Definition 10** (Sequence-Induced Distribution on States). *For a PFSA  $G = (Q, \Sigma, \delta, \tilde{\pi})$  and a distribution  $\rho_0$  on  $Q$ , the **distribution on  $Q$  induced by a sequence  $x$**  is given by  $\rho_{G, \rho_0}^T(x) = [\rho_0^T \Gamma_x]$  with  $\rho_{G, \rho_0}(\lambda) = \rho_0$ . The entry indexed by  $q \in Q$  of the vector  $\rho_{G, \rho_0}(x)$  is written as  $\rho_{G, \rho_0}(x, q)$ . When  $\rho_0 = \rho_G$ , the stationary distribution of  $G$ , we write  $\rho_{G, \rho_0}(x)$  as  $\rho_G(x)$ , or simply as  $\rho(x)$ , if  $G$  is understood.*

**Definition 11** (Stochastic Process Generated by a PFSA). *Let  $G = (Q, \Sigma, \delta, \tilde{\pi})$  be a PFSA and let  $\rho_0$  be a distribution on  $Q$ , the  $\Sigma$ -valued stochastic process  $\{X_t\}_{t \in \Sigma}$  generated by  $G$  and  $\rho_0$  satisfies that  $X_1$  follows the distribution  $\rho_0$  and  $X_{t+1}$  follows the distribution  $\rho_{G, \rho_0}(X_1 \cdots X_t)$  for  $t \in \mathbb{N}$ .*

For the rest of this paper, we will assume  $\rho_0 = \rho_G$  if not specified otherwise. We can show that, when initialized with  $\rho_G$ , the process generated by a PFSA  $G$  is stationary and ergodic. We also note the, for the process generate by  $G$ , we have  $\phi_x = \rho_G(x)^T \tilde{\Pi}$ . Since  $\rho_G(\lambda) = \rho_G$ , the symbolic derivative of the empty sequence  $\phi_\lambda$  is the stationary distribution on the symbols.

**Definition 12** (Synchronizable PFSA and Synchronizing Sequence). *A **synchronizing sequence** is a finite sequence that sends an arbitrary state of the PFSA to a fixed state<sup>32</sup>. To be more precise, let  $G = (Q, \Sigma, \delta, \tilde{\pi})$  be a PFSA, we say a sequence  $x \in \Sigma^*$  is a **synchronizing sequence** to a state  $q \in Q$  if  $\delta(q', x) = q$  for all  $q' \in Q$ . A PFSA is **synchronizable** if it has at least one synchronizing sequence. Given a sample path generated by a PFSA, we say the PFSA is **synchronized** if a synchronizing sequence transpires in the sample path.*

**Definition 13** (Equivalence and Irreducibility). *Two PFSA  $G$  and  $H$  are **equivalent** if they generate the same stochastic process. A PFSA  $G$  is said to be **irreducible**, if there is not another PFSA with smaller state set that is equivalent to  $G$ .*

**Definition 14.** Consider a PFSA  $G$  over state set  $Q$ . For a give  $\varepsilon > 0$ , we say a sequence  $x$  is a  $\varepsilon$ -synchronizing sequence to a state  $q \in Q$  if

$$\|\rho_G(x) - e_q\|_\infty \leq \varepsilon. \quad (23)$$

While there exists PFSA that is not synchronizable, we can show that an irreducible PFSA always has an  $\varepsilon$ -synchronizing sequence for some state  $q$  for arbitrarily small  $\varepsilon > 0$ . Moreover, we can show that as length increases, sequences produced by PFSA become uniformly  $\varepsilon$ -synchronizing. These two are the underpinning properties for the inference algorithm of PFSA (See Alg. 3), because they imply that  $\phi_x$  can be used to approximate  $\tilde{\pi}(q)$  if  $x$  are properly prefixed and long enough.

**Definition 15** (Joint  $\varepsilon$ -Synchronizing Sequence). *Let  $G$  and  $H$  be two PFSA over state sets  $Q_G$  and  $Q_H$ , respectively. For a fixed  $\varepsilon$ , a sequence  $x$  is said to be **jointly  $\varepsilon$ -synchronizing** to  $(q, r) \in Q_G \times Q_H$  if  $x$  is  $\varepsilon$ -synchronizing to  $q$  and to  $r$  simultaneously. We define*

$$\Sigma_{\varepsilon, (q, r)}^d \triangleq \{x \in \Sigma^d : x \text{ jointly } \varepsilon\text{-synchronizing to } (q, r)\} \quad (24)$$

**Definition 16** (Joint Pair of States). *Let  $G$  and  $H$  be two PFSA over state sets  $Q_G$  and  $Q_H$ , respectively. Define*

$$p_G(q, r) \triangleq \lim_{d \rightarrow \infty} p_G(\Sigma_{\varepsilon, (q, r)}^d) \quad (25)$$

A pair of states  $(q, r) \in Q_G \times Q_H$  is called a  **$G$ -joint pair of states** if  $p_G(q, r) > 0$ . We also define

$$Q_c \triangleq \{(q, r) \in Q_G \times Q_H : (q, r) \text{ is a } G\text{-joint pair}\} \quad (26)$$

The inference algorithm for PFSA is called **GenESS** for Generator Extraction Using Self-similar Semantics. With an input sequence  $x$  and a hyperparameter  $\varepsilon$ , **GenESS** outputs a PFSA in the following three steps: 1) approximate an almost synchronizing sequence; 2) identify the transition structure of the PFSA; 3) calculate the transition probabilities of the PFSA. See Alg. 3 for detail.

## 12. Sequence Likelihood Defect

**Definition 17** (Entropy Rate and KL Divergence). *By entropy rate of a PFSA, we mean the entropy rate of the stochastic process generated by the PFSA<sup>33</sup>. Similarly, by KL divergence of two PFSA, we mean the KL divergence between the two processes generated by them<sup>34</sup>. More precisely, we have*

$$\mathcal{H}(G) = - \lim_{d \rightarrow \infty} \frac{1}{d} \sum_{x \in \Sigma^d} p(x) \log p(x) \quad (27)$$

**Algorithm 3: GenESeSS**


---

**Data:** A sequence  $x$  over alphabet  $\Sigma$ ,  $0 < \varepsilon < 1$   
**Result:** State set  $Q$ , transition map  $\delta$ , and transition probability  $\tilde{\pi}$

```

/* Step One: Approximate  $\varepsilon$ -synchronizing sequence */
```

- 1 Let  $L = \lceil \log_{|\Sigma|} 1/\varepsilon \rceil$ ;
- 2 Calculate the **derivative heap**  $D_\varepsilon^x$  equaling  $\left\{ \hat{\phi}_y^x : y \text{ is a sub-sequence of } x \text{ with } |y| \leq L \right\}$ ;
- 3 Let  $\mathcal{C}$  be the convex hull of  $D_\varepsilon^x$ ;
- 4 Select  $x_0$  with  $\hat{\phi}_{x_0}^x$  being a vertex of  $\mathcal{C}$  and has the highest frequency in  $x$ ;

```

/* Step Two: Identify transition structure */
```

- 5 Initialize  $Q = \{q_0\}$ ;
- 6 Associate to  $q_0$  the **sequence identifier**  $x_{q_0}^{\text{id}} = x_0$  and the probability vector  $d_{q_0} = \hat{\phi}_{x_0}^x$ ;
- 7 Let  $\tilde{Q}$  be the set of states that are just added and initialize it to be  $Q$ ;
- 8 **while**  $\tilde{Q} \neq \emptyset$  **do**
  - 9 Let  $Q_{\text{new}} = \emptyset$  be the set of new states;
  - 10 **for**  $(q, \sigma) \in \tilde{Q} \times \Sigma$  **do**
    - 11 Let  $x = x_q^{\text{id}}$  and  $d = \hat{\phi}_{x\sigma}^x$ ;
    - 12 **if**  $\|d - d_{q'}\|_\infty < \varepsilon$  **for some**  $q' \in Q$  **then**
      - 13 Let  $\delta(q, \sigma) = q'$ ;
    - 14 **else**
      - 15 Let  $Q_{\text{new}} = Q_{\text{new}} \cup \{q_{\text{new}}\}$  and  $Q = Q \cup \{q_{\text{new}}\}$ ;
      - 16 Associate to  $q_{\text{new}}$  the sequence identifier  $x_{q_{\text{new}}}^{\text{id}} = x\sigma$  and the probability vector  $d_{q_{\text{new}}} = d$ ;
      - 17 Let  $\delta(q, \sigma) = q_{\text{new}}$ ;
  - 18 Let  $\tilde{Q} = Q_{\text{new}}$ ;
- 19 Take a strongly connected subgraph of the labeled directed graph defined by  $Q$  and  $\delta$ , and denote the vertex set of the subgraph again by  $Q$ ;

```

/* Step Three: Identify transition probability */
```

- 20 Initialize counter  $N[q, \sigma]$  for each pair  $(q, \sigma) \in Q \times \Sigma$ ;
- 21 Choose a random starting state  $q \in Q$ ;
- 22 **for**  $\sigma \in x$  **do**
  - 23 Let  $N[q, \sigma] = N[q, \sigma] + 1$ ;
  - 24 Let  $q = \delta(q, \sigma)$ ;
- 25 Let  $\tilde{\pi}(q) = \llbracket (N[q, \sigma])_{\sigma \in \Sigma} \rrbracket$ ;
- 26 **return**  $Q, \delta, \tilde{\pi}$ ;

---

and the KL divergence

$$\mathcal{D}_{KL}(G \parallel H) = \lim_{d \rightarrow \infty} \frac{1}{d} \sum_{x \in \Sigma^d} p_G(x) \log \frac{p_G(x)}{p_H(x)} \quad (28)$$

whenever the limits exist.

**Theorem 1** (Closed-form Formula for Entropy Rate and KL Divergence). *The entropy rate of a PFSA  $G = (\Sigma, Q, \delta, \tilde{\pi})$  is given by*

$$\mathcal{H}(G) = \sum_{q \in Q} \wp_G(q) \cdot h(\tilde{\pi}(q)) \quad (29)$$

where  $h(v)$  is the based-2 entropy of the probability vector  $v$ .

Consider two PFSA  $G = (Q_G, \Sigma, \delta_G, \tilde{\pi}_G)$  and  $H = (Q_H, \Sigma, \delta_H, \tilde{\pi}_H)$  with  $\mu_G$  being absolutely continuous with respect to  $\mu_H$ . Let  $Q_c$  be the set of  $G$ -joint pairs of states, we have

$$\mathcal{D}_{KL}(G \parallel H) = \sum_{(q, r) \in Q_c} p_G(q, r) \mathcal{D}_{KL}(\tilde{\pi}_G(q) \parallel \tilde{\pi}_H(r)) \quad (30)$$

**Definition 18** (Log-likelihood). *Let  $x \in \Sigma^d$ , the log-likelihood<sup>33</sup> of a PFSA  $G$  generating  $x$  is given by*

$$L(x, G) = -\frac{1}{d} \log p_G(x) \quad (31)$$

The calculation of log-likelihood is detailed in Alg. 4.

---

**Algorithm 4:** Log-likelihood

---

**Data:** A PFSA  $G = (\Sigma, Q, \delta, \tilde{\pi})$  and a sequence  $x$  over alphabet  $\Sigma$   
**Result:** Log-likelihood  $L(x, G)$  of  $G$  generating  $x$

- 1 Calculate the state transition matrix  $\Pi$  and observation  $\tilde{\Pi}$ ;
- 2 Calculate the stationary distribution over states  $\varphi_G$  of  $G$  from  $\Pi$ ;
- 3 Calculate the stationary distribution of alphabet  $\phi_\lambda^T = \varphi_G^T \tilde{\Pi}$ ;
- 4 Initialize  $p$  by  $\varphi_G$  and  $q$  by  $\phi_\lambda$ ;
- 5 Let  $L = 0$ ;
- 6 **for**  $i$  from 1 to  $|x|$  **do**
- 7   Let  $\sigma$  be the  $i$ -th entry of  $x$ ;
- 8   Let  $L = L - \log q|_\sigma$ ;
- 9   Let  $p^T = [\![p^T \Gamma_\sigma]\!]$  where  $\Gamma_\sigma$  is defined in 9;
- 10   Let  $q^T = p^T \tilde{\Pi}$ ;
- 11 **return**  $L/|x|$ ;

---

**Theorem 2** (Convergence of log-likelihood). *Let  $G$  and  $H$  be two reduced PFSA, and let  $x \in \Sigma^d$  be a sequence generated by  $G$ . Then we have*

$$L(x, H) \rightarrow \mathcal{H}(G) + \mathcal{D}_{KL}(G \parallel H) \quad (32)$$

in probability as  $d \rightarrow \infty$ .

*Proof.* We first notice that

$$\sum_{x \in \Sigma^d} p_G(x) \log \frac{p_G(x)}{p_H(x)} = \sum_{x \in \Sigma^{d-1}} \sum_{\sigma \in \Sigma} p_G(x) \varphi_G(x) \tilde{\Pi}_G \Big|_\sigma \log \frac{p_G(x) \varphi_G(x) \tilde{\Pi}_G \Big|_\sigma}{p_H(x) \varphi_H(x) \tilde{\Pi}_H \Big|_\sigma} \quad (33)$$

$$= \sum_{x \in \Sigma^{d-1}} p_G(x) \log \frac{p_G(x)}{p_H(x)} + \underbrace{\sum_{x \in \Sigma^{d-1}} p_G(x) \sum_{\sigma \in \Sigma} \varphi_G(x) \tilde{\Pi}_G \Big|_\sigma \log \frac{\varphi_G(x) \tilde{\Pi}_G \Big|_\sigma}{\varphi_H(x) \tilde{\Pi}_H \Big|_\sigma}}_{D_d} \quad (34)$$

By induction, we have  $\mathcal{D}_{KL}(G \parallel H) = \lim_{d \rightarrow \infty} \frac{1}{d} \sum_{i=1}^d D_i$ , and hence by Cesàro summation theorem<sup>35</sup>, we have  $\mathcal{D}_{KL}(G \parallel H) = \lim_{d \rightarrow \infty} D_d$ . Let  $x = \sigma_1 \sigma_2 \dots \sigma_n$  be a sequence generated by  $G$ . Let  $x^{[i-1]}$  is the truncation of  $x$  at the  $(i-1)$ -th symbols, we have

$$-\frac{1}{n} \sum_{i=1}^n \log \varphi_H(x^{[i-1]}) \tilde{\Pi}_H \Big|_{\sigma_i} = \underbrace{\frac{1}{n} \sum_{i=1}^n \log \frac{\varphi_G(x^{[i-1]}) \tilde{\Pi}_G \Big|_{\sigma_i}}{\varphi_H(x^{[i-1]}) \tilde{\Pi}_H \Big|_{\sigma_i}}}_{A_{x,n}} - \underbrace{\frac{1}{n} \sum_{i=1}^n \log \varphi_G(x^{[i-1]}) \tilde{\Pi}_G \Big|_{\sigma_i}}_{B_{x,n}} \quad (35)$$

Since the stochastic process  $G$  generates is ergodic, we have

$$\lim_{n \rightarrow \infty} A_{x,n} = \lim_{d \rightarrow \infty} D_d = \mathcal{D}_{KL}(G \parallel H) \quad (36)$$

and  $\lim_{n \rightarrow \infty} B_{x,n} = \mathcal{H}(G)$ .  $\square$

## References

- [1] Guthrie, W. *et al.* Accuracy of Autism Screening in a Large Pediatric Network. *Pediatrics* **144** (2019).
- [2] Chattopadhyay, I. & Lipson, H. Abductive learning of quantized stochastic processes with probabilistic finite automata. *Philos Trans A* **371**, 20110543 (2013).
- [3] Breiman, L. Random forests. *Mach. Learn.* **45**, 5–32 (2001).
- [4] Friedman, J. H. Stochastic gradient boosting. *Comput. Stat. Data Anal.* **38**, 367–378 (2002).
- [5] Hochreiter, S. & Schmidhuber, J. Long short-term memory. *Neural Comput.* **9**, 1735–1780 (1997).
- [6] Gordon-Lipkin, E., Foster, J. & Peacock, G. Whittling down the wait time: exploring models to minimize the delay from initial concern to diagnosis and treatment of autism spectrum disorder. *Pediatric Clinics* **63**, 851–859 (2016).
- [7] Penner, M., Anagnostou, E. & Ungar, W. J. Practice patterns and determinants of wait time for autism spectrum disorder diagnosis in canada. *Molecular autism* **9**, 16 (2018).

- [8] Hyman, S. L., Levy, S. E., Myers, S. M. et al. Identification, evaluation, and management of children with autism spectrum disorder. *Pediatrics* **145** (2020).
- [9] Johnson, C. P., Myers, S. M. et al. Identification and evaluation of children with autism spectrum disorders. *Pediatrics* **120**, 1183–1215 (2007).
- [10] Zwaigenbaum, L. et al. Early intervention for children with autism spectrum disorder under 3 years of age: recommendations for practice and research. *Pediatrics* **136**, S60–S81 (2015).
- [11] Robins, D. L. et al. Validation of the modified checklist for autism in toddlers, revised with follow-up (m-chat-r/f). *Pediatrics* **133**, 37–45 (2014).
- [12] Esler, A. N. et al. The autism diagnostic observation schedule, toddler module: standardized severity scores. *Journal of Autism and Developmental Disorders* **45**, 2704–2720 (2015).
- [13] Chlebowski, C., Green, J. A., Barton, M. L. & Fein, D. Using the childhood autism rating scale to diagnose autism spectrum disorders. *Journal of autism and developmental disorders* **40**, 787–799 (2010).
- [14] Falkmer, T., Anderson, K., Falkmer, M. & Horlin, C. Diagnostic procedures in autism spectrum disorders: a systematic literature review. *European child & adolescent psychiatry* **22**, 329–340 (2013).
- [15] Lord, C. et al. Autism from 2 to 9 years of age. *Archives of general psychiatry* **63**, 694–701 (2006).
- [16] Kleinman, J. M. et al. Diagnostic stability in very young children with autism spectrum disorders. *Journal of autism and developmental disorders* **38**, 606–615 (2008).
- [17] Bolton, P. F., Golding, J., Emond, A. & Steer, C. D. Autism spectrum disorder and autistic traits in the avon longitudinal study of parents and children: precursors and early signs. *Journal of the American Academy of Child & Adolescent Psychiatry* **51**, 249–260 (2012).
- [18] Kozlowski, A. M., Matson, J. L., Horovitz, M., Worley, J. A. & Neal, D. Parents' first concerns of their child's development in toddlers with autism spectrum disorders. *Developmental neurorehabilitation* **14**, 72–78 (2011).
- [19] Baio, J. Prevalence of autism spectrum disorder among children aged 8 years—autism and developmental disabilities monitoring network, 11 sites, united states, 2010 (2014).
- [20] Kalb, L. G. et al. Determinants of appointment absenteeism at an outpatient pediatric autism clinic. *Journal of Developmental & Behavioral Pediatrics* **33**, 685–697 (2012).
- [21] Bisgaier, J., Levinson, D., Cutts, D. B. & Rhodes, K. V. Access to autism evaluation appointments with developmental-behavioral and neurodevelopmental subspecialists. *Archives of pediatrics & adolescent medicine* **165**, 673–674 (2011).
- [22] Fenikilé, T. S., Ellerbeck, K., Filippi, M. K. & Daley, C. M. Barriers to autism screening in family medicine practice: a qualitative study. *Primary health care research & development* **16**, 356–366 (2015).
- [23] Althouse, L. A. & Stockman, J. A. Pediatric workforce: A look at pediatric nephrology data from the american board of pediatrics. *The Journal of pediatrics* **148**, 575–576 (2006).
- [24] Hopcroft, J. E. *Introduction to automata theory, languages, and computation* (Pearson Education India, 2008).
- [25] Klenke, A. *Probability theory: a comprehensive course* (Springer Science & Business Media, 2013).
- [26] Doob, J. *Stochastic processes*. Wiley publications in statistics (Wiley, 1990). URL <https://books.google.com/books?id=7Bu8jgEACAAJ>.
- [27] Chattopadhyay, I. & Ray, A. Structural transformations of probabilistic finite state machines. *International Journal of Control* **81**, 820–835 (2008).
- [28] Chattopadhyay, I. & Lipson, H. Data smashing: uncovering lurking order in data. *Journal of The Royal Society Interface* **11**, 20140826 (2014).
- [29] Bondy, J. & Murty, U. Graph theory (2008). *Grad. Texts in Math* (2008).
- [30] Vidyasagar, M. *Hidden markov processes: Theory and applications to biology*, vol. 44 (Princeton University Press, 2014).
- [31] Kai, L. C. *Markov Chains: With Stationary Transition Probabilities* (Springer-Verlag, 1967).
- [32] Trahtman, A. N. The road coloring and Černý conjecture. In *Proc. of Prague stringology conference*, vol. 1, 12 (Citeseer, 2008).
- [33] Cover, T. M. & Thomas, J. A. *Elements of information theory* (John Wiley & Sons, 2012).
- [34] Matthews, A. G. d. G., Hensman, J., Turner, R. & Ghahramani, Z. On sparse variational methods and the kullback-leibler divergence between stochastic processes. *Journal of Machine Learning Research* **51**, 231–239 (2016).
- [35] Hardy, G. Divergent series, with a preface by J. E. Littlewood and a note by G. H. Hardy, reprint of the revised (1963) edition. *Éditions Jacques Gabay, Sceaux* (1992).